Assessing placental function across gestation: a multi-institutional study of BOLD-MRI for the prediction of adverse pregnancy outcomes

Matthias Schabel
Oregon Health & Science University
Victoria Roberts
Oregon National Primate Research Center
Karen Gibbins
Oregon Health and Science University
Monica Rincon
Oregon Health and Science University
Jessica Gaffney
Oregon Health and Science University
Aaron Streblow
Oregon Health and Science University
Adam Wright
Oregon Health and Science University https://orcid.org/0000-0001-9524-2210
Jaime Lo
Oregon Health & Science University
Byung Park
Oregon Regional Primate Center
Christopher Kroenke
Oregon Health & Science University https://orcid.org/0000-0001-7398-3632
Kathryn Szczotka
University of Utah
Nathan Blue
University of Utah
Jessica Page
University of Utah
Kathy Harvey
University of Utah
Michael W. Varner
University of Utah School of Medicine
Robert Silver

University of Utah
Antonio Frias (friasa@ohsu.edu)
ONPRC/OHSU

Article

Keywords: Maternal-fetal Interactions, Fetal Development, Placental Dysfunction, Pregnant Non-human Primate, Maternal-fetal Oxygen Transport

Posted Date: April 26th, 2021

DOI: https://doi.org/10.21203/rs.3.rs-406266/v1

Assessing placental function across gestation: a multi-institutional study of BOLD-MRI for the prediction of adverse pregnancy outcomes**.**

Matthias C Schabel, PhD[1#*], Victoria HJ Roberts, PhD[2#], Karen J Gibbins, MD[3#], Monica Rincon, MD[3], Jessica E Gaffney, BS[2], Aaron D Streblow, BS[2], Adam M Wright, BS[2], Jamie O Lo, MD[3], Byung Park, PhD[4], Christopher D Kroenke, PhD[1,5], Kathryn Szczotka, MPH[6], Nathan R Blue, MD[6], Jessica M Page, MD[6], Kathy Harvey, BS[6], Michael W Varner, MD[6], Robert M Silver, MD[6], Antonio E Frias, MD[2,3*]

[1]Advanced Imaging Research Center, Oregon Health and Science University (OHSU)

[2]Division of Reproductive and Developmental Sciences, Oregon National Primate Research Center (ONPRC), OHSU

[3]Department of Obstetrics and Gynecology, OHSU

[4]Biostatistics Shared Resource, Knight Cancer Institute, OHSU

[5]Division of Neuroscience, ONPRC, OHSU

[6]Department of Obstetrics and Gynecology, University of Utah

*Corresponding authors

[#]Joint first authors

Abstract

The placenta is a remarkable organ that coordinates and regulates maternal-fetal interactions during pregnancy to optimize fetal development. A host of obstetric complications are associated with placental dysfunction, and existing methods for evaluating *in vivo* placental function fail to reliably detect at-risk pregnancies prior to maternal or fetal morbidity. Although routinely used as a monitoring tool, the predictive power of ultrasound for identifying compromised pregnancies is poor. Recent preclinical studies performed in our laboratory, using blood oxygen-level dependent magnetic resonance imaging (BOLD-MRI) in the pregnant nonhuman primate (NHP), established a strong correlation between placental T2* values and maternal-fetal oxygen transport. Here we extend this work to a large, longitudinal, two-site study of quantitative *in vivo* T2* mapping in human pregnancies across 11 to 38 weeks gestation to characterize the evolution of placental oxygenation in uncomplicated pregnancies and to elucidate the relationship between aberrant placental T2* and adverse obstetric outcomes attributable to placental dysfunction. This methodology has high discriminatory power and strong potential diagnostic utility.

Introduction

The fundamental role of the placenta in fetal development, pregnancy morbidity, and neonatal, pediatric, and even lifelong health is indisputable (1-7). Aberrant placental development has been linked to virtually every adverse obstetric outcome, including abnormalities in fetal growth, preeclampsia, preterm labor, and stillbirth (4, 8-17). During pregnancy, the placenta supplies oxygen and critical nutrients required for fetal growth, removes waste products from the fetal circulation, protects the fetus from environmental toxins and infections, produces pregnancy-specific hormones, and mediates communication between the fetus and the mother to coordinate maternal physiologic adaptations and fetal development (18-20). The regulation of all of these processes changes dynamically across gestation to ensure appropriate maternal resource allocation to meet fetal growth demands. Although mechanisms regulating normal placental growth and development are incompletely understood, the central role of the placenta in fetal homeostasis is clear.

The inability to longitudinally sample placental tissue during gestation constitutes a significant limitation for the study and *assessment* of placental development in human pregnancies. Therefore, development of non-invasive tools and diagnostics to accurately characterize normal

development across gestation and assess placental function and health *in vivo* is a crucial component in the identification of pregnancies at risk for adverse obstetric and neonatal outcomes.

Obstetric imaging, predominantly with ultrasound (US), is a mainstay of clinical care for identification of fetal anomalies and detection of aberrant fetal growth (21-25). Uterine artery velocimetry has been studied as a potential predictor of preeclampsia and fetal growth restriction (FGR), and has modest predictive power for severe, early onset phenotypes of both (22, 24, 26), but it performs poorly in predicting later onset morbidity due to placental dysfunction, possibly because it measures resistance to blood flow (impedance) in the umbilical artery rather than focusing on perfusion of the placenta itself (27). Similarly, fetal umbilical artery Doppler ultrasound is used to risk stratify pregnancies suspected to have FGR based on ultrasound fetal biometry. Observation of abnormal blood flow via umbilical artery Doppler assessment, particularly absent or reversed diastolic blood flow, is clearly associated with adverse perinatal outcomes (28, 29). However, its principal utility is in antenatal surveillance to guide hospitalization and timing of delivery after the diagnosis of FGR has already been established by ultrasound-based biometry, not in prediction of incipient FGR. Although it is clear that profoundly abnormal umbilical artery blood flow in the setting of FGR is associated with adverse perinatal outcome (28), it is not a direct measure of placental function and it can be normal in some cases of severe placental insufficiency. Despite its widespread use, the utility of screening ultrasound as a tool for identification of pregnancies at risk for adverse outcomes remains limited.

Magnetic resonance imaging (MRI) has been used during pregnancy for decades, primarily to assess fetal abnormalities via anatomic imaging. Recently, the NIH Human Placenta Project stimulated the development and application of a number of innovative MRI techniques, intended to enable *in vivo* assessment of placental function during pregnancy (30). Early work by Sorensen and colleagues (31) observed the presence of spatial heterogeneity in T2*-weighted MRI of the placenta, and found that this heterogeneity was decreased by maternal hyperoxia. It is well-known that T2*-weighted images are sensitive to changes in the relative levels of oxyhemoglobin and deoxyhemoglobin via the blood oxygenation level dependent (BOLD) effect, which forms the basis of functional MRI (fMRI) studies of the brain (32). Consideration of the specifics of the anatomy and physiology of hemochorial placentas led us to hypothesize that quantitative T2* measurements could be used to assess placental perfusion and maternal-fetal oxygen transport. Subsequent work performed by our group in pregnant nonhuman primates

(NHPs), combining dynamic contrast enhanced (DCE-) MRI with quantitative T2* mapping (33, 34) proved that the observed heterogeneity in placental T2* arises from spatial gradients in maternal placental blood (MPB) oxygen saturation within functional lobules. We then developed a simple model based on relevant physiological parameters of the placenta that accounts for these spatial variations. Highly oxygenated maternal blood delivered to the placenta via spiral arteries has large T2* values that decrease continuously toward the placental lobular margins as oxygen from the MPB is extracted by the villi and transported to the fetus. This research demonstrates that T2* relaxometry provides a measure of the critical balance between maternal supply of oxygen to the fetal vasculature and fetal uptake of the supplied oxygen. Recent NHP studies from our group have further shown that anomalous baseline T2* values are correlated with placental dysfunction in cases of fetal growth restriction as well as secondary to perturbations with prenatal alcohol exposure or Zika virus infection (35-37).

Placental T2* has been measured throughout gestation in both uncomplicated human pregnancies and human pregnancies with adverse outcomes by a number of groups (38-44). These studies verified that placental T2* decreases with gestational age, consistent with results from NHP studies and with the expected effect of increased fetal oxygen demand with growth. Given the direct association between T2* and maternal-fetal oxygen transport, it is conceivable that this non-invasive MRI measure could be applicable to clinical studies of placental function. However, the paucity of longitudinal data, incorporation of specialized image acquisition or analysis procedures, and minimal experience comparing data between sites limit our current ability to extend T2* measurements to large-scale studies.

Based on preliminary evidence in NHP and human pregnancies, we hypothesized that placental T2* values in pregnancies complicated by clinical placental dysfunction would be lower for gestational age compared to uncomplicated pregnancies as a result of inadequate maternal oxygen supply to the placenta. The primary objective of this work was to test this hypothesis by conducting a prospective, longitudinal, two-site MRI study in 316 pregnant women, with intentional population enrichment for obstetric morbidity due to placental dysfunction. A secondary objective was to establish whether data acquired at two different institutions, using compatible scanner hardware and MRI protocols and analyzed by uniform post processing, would demonstrate sufficient data consistency to support conducting larger multi-institutional studies of this non-invasive imaging method to identify and assess placentally-mediated adverse pregnancy outcomes.

Results

Participant and study demographics

Details of participant enrollment and study completion at the two study sites are presented in the flow chart in Figure 1. Demographics and maternal characteristics are detailed in Table 1. MRI data of adequate quality to perform T2* analysis were acquired in 797 imaging studies from 316 individual study participants (450 scans from 179 participants at OHSU, 347 scans from 137 participants at Utah). At least one usable MRI scan was obtained from 86% of participants who were consented (88% at OHSU, 83% at Utah), with all three scans completed in 66% of these patients, two scans in 20%, and a single scan in 14%. Of these studies, 700 had usable hemoglobin data (426 at OHSU, 274 at Utah) and 432 had usable SpO2 measurements (252 at OHSU, 180 at Utah). 352 usable quantitative T1 measurements were also obtained in 156 of the OHSU participants.

Pregnancy outcomes

Out of 316 participants, 198 (62.6%) were classified as uncomplicated pregnancies (UN), 70 (21.8%) were classified in the primary adverse (PA) outcome group, and 48 (15.2%) were classified in the secondary abnormal (SA) outcome group, as defined in the Methods. Within primary adverse outcome group, the most commonly observed component was preeclampsia with severe features (40.0%) followed by gestational hypertension (31.4%), and small for gestational age (SGA, 20.0%) (Table 2). Both severe pre-eclampsia and SGA were more prevalent in the OHSU cohort than the Utah cohort, but the observed differences were not statistically significant on chi-square test. 35.7% of those with the primary adverse outcome delivered prior to 37 weeks, our threshold for prematurity.

Birthweight statistics

Median birthweight percentile (computed using the tables from Oken (45)) was 48.2 in UN pregnancies, 32.7 in PA pregnancies, and 48.8 in the SA pregnancies. There was a significant difference in birthweight percentile between UN and PA outcome groups (p=0.017) but not between UN and SA (p=0.28). When stratified by study site, birthweight percentiles for UN, PA, and SA were 50.5, 30.3, and 49.3 at OHSU, and 42.0, 36.1, and 46.5 at Utah, respectively. Birthweight was significantly lower in PA vs. UN outcome groups in the OHSU cohort (p=0.023) but not at Utah (p=0.42). There was no difference between UN and SA outcome groups at either site (OHSU p=0.74, Utah p=0.51).

*Placental T2**

Figure 2 shows representative anatomic T2-weighted HASTE (left column) and quantitative T2* maps (right column) acquired in two study participants, matched for gestational age at time of scan. Placental regions of interest (ROIs) are superimposed on the T2* maps (blue dashed lines). The upper row in the figure shows a UN pregnancy at 232 days of gestation with median placental T2* (= 51 ms) close to the population median (50^{th} percentile), while the bottom row shows corresponding images for a PA pregnancy at 235 days gestation with a median T2* (= 26 ms) in the 1^{st} percentile. Depression of the placental T2* in the latter is clearly apparent in panel D.

Figure 3A shows the measured dependence of placental T2* across gestation in UN pregnancies. This quantity decreased continuously throughout pregnancy, beginning at a relatively high plateau level early in gestation, then dropping increasingly rapidly to an inflection point around 30 weeks before approaching a second, lower plateau in late gestation. Model fitting via nonlinear least squares regression to a logistic function is shown by the solid black curve, with 95% fit confidence intervals (CI) indicated by the dashed lines and 95% fit prediction intervals (PI) by the dot-dashed lines. Figure 3B plots the corresponding data and regression curves for SA (green) and PA (red) pregnancies, with the best fit and 95% CI curves from UN pregnancies shown in gray for reference. The model fit for the PA outcome group had significantly lower modeled T2* than UN pregnancies starting at 15 weeks and continuing through 33 weeks gestation, while the model fit for the SA outcome group was not significantly different from that for UN pregnancies at any point in gestation.

Site-dependent data and regressions for UN pregnancies are shown in Figure 3C for OHSU (blue) and Utah (red), with fit and 95% CI for all UN again plotted in gray. While the resulting curves are quite similar in shape, the Utah T2* data for UN pregnancies are consistently lower than the corresponding OHSU data, and the difference between the two is statistically significant between 15 and 29 weeks gestation. The observed site-specific differences in T2* in UN placentas can be accurately described with a simple model (see Methods) that characterizes these differences in terms of corresponding site differences in maternal hemoglobin and SpO2 levels, the known dependence of MRI signal on deoxyhemoglobin concentration, and a gestation-dependent maternal placental blood volume fraction ($v_{mpb}(t)$) term that varies from approximately 15% early in gestation to approximately 35% by late gestation. Hemoglobin and SpO2 variation between imaging sites can be explained by the

altitude difference, with the University of Utah at 4,840 feet above sea level while OHSU lies roughly 450 feet above sea level.

Median voxel-level relative measurement uncertainty in placental T2* data for UN pregnancies was ±7.0%, was comparable in both SA (±6.1%) and PA (±6.2%) pregnancies, and was significantly higher in the Utah studies than at OHSU (±5.8% for OHSU, 10.3% for Utah, $p<0.001$). In addition to stratifying based on pregnancy outcome and study site, the dependence of gestational T2* measurements in UN pregnancies on fetal sex, maternal age, and maternal body mass index (BMI) was evaluated (not plotted), with no significant differences among any of these. Excluding measurements not meeting the heuristic data quality criteria described in the methods did not significantly alter any reported results.

The average rate of change in placental T2* with gestation, computed from the centered finite difference of measurements in each individual pregnancy at successive time points, is plotted for UN pregnancies in Figure 3D, for PA (red), and SA (green) pregnancies in Figure 3E, and for OHSU (blue) vs. Utah (red) UN in Figure 3F. Model regressions to these data using the time derivative of the logistic function are displayed as in Figures 3A-3C. As with the T2* data themselves, the rate of change data for UN and SA pregnancies are not significantly different at any point during gestation. In contrast, the rate of change in PA pregnancies is nearly constant and shows a significantly larger rate of decrease in early and mid-gestation (up to 24 weeks) relative to UN. The rate of T2* decrease with gestation was found to be slightly, but significantly, larger in OHSU UN pregnancies than in Utah UN from 28 weeks gestation onward.

*Receiver operating characteristic (ROC) curves for T2**

Histograms of T2* z-values for uncomplicated normal (blue), primary adverse outcome (red), and secondary abnormal outcome pregnancies (green) are plotted in Figure 4, where the uncomplicated pregnancies were used as the reference distribution. As expected, the distribution of z-scores for UN pregnancies is symmetrical and centered on zero (mean=0.0, SD=1.0). Z-scores for the PA pregnancies are relatively symmetrical but broader and with a significant left shift (mean=-1.0, SD=1.49, $p<0.001$), while the distribution for SA pregnancies is shifted leftward (mean=-0.15, SD=1.34, $p<0.001$) and notably skewed, suggesting the possibility of two subpopulations within these data.

The distributions of T2* percentiles derived from the z-score data are presented in bar chart form in Figure 5, with twenty equally-spaced bins spanning from 0 to 100. The distribution of T2* percentiles in the UN population (blue) is, as expected, essentially uniform across the entire

range, with roughly 5% of observations lying in each bin, while SA (green) pregnancies show modest enrichment at low values. In contrast, the PA pregnancies lie primarily in the lowest (0-5%) bin, with nearly 35% of the adverse studies lying in that range and 44% in the lowest 10% of T2* measurements.

Figure 6 shows receiver operating characteristic (ROC) curves for the entire population across gestation (leftmost column), and for data separated into early (10-20 weeks), mid (20-30 weeks), and late (30+ weeks) gestation (second through fourth columns). ROCs for both sites are plotted in the top row, those computed using only OHSU data in the middle row, and those computed using only the Utah data in the bottom row. For both sites across all gestational time points, the area under the curve (AUC) or C-statistic for placental T2* and PA pregnancy outcome is 0.71, with mid-gestation showing the strongest predictive power (AUC of 0.76). C-statistics are consistently higher in the OHSU cohort than the Utah cohort, with the strongest C-statistic overall for OHSU studies in mid-gestation (AUC=0.82), and the weakest for Utah studies in late-gestation (AUC=0.37). The maximum in Youden's J statistic, J_{max}, is indicated by the red stars on the ROC curves of Figure 6, and the corresponding optimal cutoff threshold in T2* percentile relative to UN is indicated in the legends as C_{opt}.

Placental T1

Quantitative T1 values in UN pregnancies (acquired in OHSU participants only) showed linear decrease with gestation at an average rate of -26.9 ms/week from approximately 2200 ms early in gestation to roughly 1600 ms late in gestation. Neither SA nor PA pregnancies showed any statistically significant differences in the evolution of T1 during pregnancy relative to UN, suggesting that placental T1 is not a useful metric for characterization of placental dysfunction.

Maternal hemoglobin and oxygen saturation

Maternal hemoglobin level decreased linearly throughout gestation in UN pregnancies at an average rate of -0.046 mmol/week and was significantly higher in the Utah cohort than the OHSU cohort (mean difference 1.04±0.90 mmol, $p<0.001$). Maternal hemoglobin was significantly higher in the PA pregnancies compared to UN (mean difference 0.36±1.04 mmol, $p<0.001$). There was no difference in hemoglobin between UN and SA pregnancies.

Maternal SpO2 in UN pregnancies was found to be essentially constant throughout gestation (mean 97.0%) but was significantly lower in the Utah cohort than the OHSU cohort (mean

242 difference -2.0±3.0%, p<0.001). Neither SA nor PA pregnancies were associated with
243 statistically different maternal SpO2 values or trends relative to UN.

244 *Placental volume*

245 Placental volume increased linearly during gestation at an average rate of 32.2 cm^3/week
246 beginning between 11 and 12 weeks, with no significant difference between UN pregnancies at
247 the two sites. Our placental volume measurements are also highly consistent with those
248 reported by Leon et al. (46) in the overlapping gestational age range. Volume in SA pregnancies
249 was not significantly different than that of UN, while PA pregnancies showed a slightly lower rate
250 of growth (30.0 cm^3/week) leading to significantly lower volume from 20 weeks gestation
251 onward.

252 *Regression modeling results*

253 Model definitions, best fit parameter values, fit parameter uncertainties, and root-mean-square
254 (RMS) residual errors for regressions to all data and subsets discussed above are given in
255 Table 3.

256 **Discussion**

257 In this study, we characterize and model the sigmoidal evolution of T2* across gestation in
258 uncomplicated pregnancies and demonstrate that median placental T2* is markedly lower in
259 many pregnancies with adverse outcomes. We found lower values across gestation in
260 pregnancies with the primary adverse outcome and larger rate of decline in early and mid-
261 gestation when compared to uncomplicated normal pregnancies. Importantly, decreased
262 median T2* continues to correlate with adverse obstetric outcomes when quantified in both mid
263 and late gestation. The placenta is a dynamic organ which evolves over the entire course of
264 gestation, and possesses the capacity to adaptively develop in concert with the growing fetus.
265 As a result, it is not a *fait accompli* that poor placental function early in gestation persists
266 throughout pregnancy. However, our results suggest that, while T2* measurements acquired in
267 the mid-gestational time window (20-30 weeks) are most predictive of adverse pregnancy
268 outcomes, even data from the early gestational window (10-20 weeks) allow risk stratification.

269 The strong correlation of data observed between our two independent sites demonstrates that
270 this method is robust and has the potential to be transferable across different institutions.
271 Nevertheless, some relevant site-specific differences were observed that merit further
272 clarification. First, the birthweight in PA pregnancies among the Utah group was not

significantly different from that of the UN pregnancies in that group, while the PA pregnancies in the OHSU cohort had a significantly lower birthweight when compared to UN. This may simply be accounted for by the higher proportion of SGA neonates in the OHSU cohort due to chance, as population rates of adverse outcomes in these two groups are expected to be similar. Second, the maternal Hgb was higher in Utah when compared to OHSU, which is expected given the increased altitude in Salt Lake City, Utah when compared to Portland, Oregon. Third, maternal oxygen saturation in the Utah patients was significantly lower than in the OHSU population, also consistent with the physiologic impacts of altitude. In the UN population, it is possible to entirely explain the observed differences between sites with a simple model incorporating the site-specific hemoglobin and oxygen saturation differences along with a maternal placental blood volume term that varies across gestation, as described in the Methods.

The predictive power of T2* measurements for discriminating uncomplicated pregnancies from primary adverse outcome pregnancies was much higher in the OHSU cohort than for Utah (AUC 0.80 vs 0.56). We suspect that this is due to site-specific differences in the prevalence of SGA and preeclampsia with severe features, both of which are relatively under-represented in the Utah group. Notably, in the Utah cohort, birthweights of neonates in the primary adverse outcome group were not statistically different than in uncomplicated pregnancies. Given that SGA and hypertensive diseases of pregnancy have multiple pathophysiologies with varying degrees of placental dysfunction, it is reasonable to propose that T2* quantification is primarily predictive of pathways linked to abnormalities attributable to perturbations of maternal placental blood flow and/or fetal oxygen uptake. It is possible that there is a secondary contribution due to the somewhat higher measurement error in the Utah data set as compared to OHSU, although the absolute measurement uncertainties are small for both study sites. Unfortunately, the modest number of PA pregnancies in our data set limits statistical power and precludes separation of the PA group into sub-categories.

The imaging methodology in this study is highly amenable to clinical translation. Placental MRI was performed using imaging protocols and pulse sequences that are available on virtually all modern MRI scanners, and analysis of these data requires only minimal post-processing to convert signal measurements to T2* values. Groundwork performed in our NHP models was key to both validation and translation of this methodology to human subjects by validating T2* mapping as a functional measure of maternal placental perfusion with confirmation by DCE-MRI (33, 34). While DCE-MRI is the gold-standard method for quantifying tissue perfusion via MRI, and despite the fact that we have demonstrated minimal placental permeability to passage of

gadolinium-based contrast agents (GBCA) following i*n utero* maternal administration (47, 48), a GBCA-free alternative alleviates potential reservations to use of MRI as a clinical diagnostic imaging tool for assessing placental health. In addition, because placental T2* is sensitive to the balance between oxygenated maternal blood delivery and fetal oxygen demand, it is particularly well-suited to identify problems stemming from inadequate placental oxygenation.

Study strengths and limitations

Our study has a number of strengths. It is the largest prospective study of placental MRI, and the most extensive study of T2*, in particular. In addition, the longitudinal design enabled us to characterize the nonlinear evolution of T2* across pregnancy and provide reference values for both T2* itself and rate of change in T2* as gestation progresses. While studies of changes in T2*-weighted BOLD-EPI measurements in response to hyperoxygenation have a number of advantages, particularly in data acquisition efficiency and sensitivity to motion, they are generally semi-quantitative, introduce methodological complexity, and potentially perturb maternal and fetal hemodynamics and alter the physiologic mechanisms that determine normal oxygen transport across a gradient (49-51). In contrast, quantitative measurements of T2* are reflective of the balance between maternal delivery of oxygen and fetal demand, are reproducible across sites, and do not need ancillary experimental perturbations. The primary adverse composite outcome metric we developed was defined prior to, and independent of, MRI data analysis. Designation of pregnancy outcome was blinded to MRI data analysis and was conducted by four Maternal-Fetal Medicine physicians independently, increasing the rigor of our outcome designation. Similarly, to further reduce the potential for bias, MRI data processing was blinded to pregnancy outcome and was conducted independently prior to statistical analysis for association with adverse pregnancy outcomes. By utilizing common, commercially available MRI acquisition protocols, the work described here should be easy to reproduce at other institutions, facilitating its potential use both in future clinical studies and in clinical practice.

There are also a number of limitations to this study. Although it is the largest longitudinal MRI study in pregnancy performed to date, the number of adverse outcomes was small. This necessitated the utilization of a composite outcome, as is typical for obstetric studies. Our study population is relatively ethnically and racially homogeneous, so the conclusions we draw here may not be applicable to other populations. MRI was performed using 3 Tesla scanning hardware to increase sensitivity to changes in T2*, but these systems are not currently the standard in obstetric imaging and are not as widely available as 1.5 Tesla systems. While we used consistent criteria encompassing many common complications, there is no gold standard

definition of placental dysfunction, and our outcomes are heterogenous by nature. In particular, we have previously identified circumstances where pathology related to villous inflammation or malformation can cause elevated T2* (35) in the setting of adequate supply of maternal arterial blood to the placenta in conjunction with impaired trans-villous oxygen permeability, which could constitute a confounding factor in some pregnancies. As a result, further refinement may be required to detect abnormally high, as well as abnormally low T2*, to accurately capture different types of placental pathology.

Conclusion

We present the results of a prospective longitudinal human study that demonstrate the potential of quantitative T2* mapping during pregnancy to identify increased risk for adverse obstetric outcome due to placental dysfunction, particularly in the setting of fetal growth restriction. Quantitative measures of placental T2* identified pregnancies at increased risk for adverse outcomes across all gestational ages in this study despite site-specific differences in maternal and neonatal demographics at the two institutions. Low median placental T2* was strongly correlated with low fetal birthweight, suggesting that the diagnostic utility of placental MRI may be enhanced by focusing on a specific adverse obstetric outcome, such as fetal growth restriction, rather than a composite adverse outcome. Improved diagnostics to identify pregnancies at risk of adverse outcomes may facilitate discovery of novel biomarkers, improved stratification of patients in clinical studies, and may allow for earlier modification of clinical management plans.

Methods

All protocols described in the following were approved by the Institutional Review Boards (IRB) at Oregon Health & Science University (OHSU) and University of Utah Health Sciences Center (UUHSC), and study oversight was provided by an independent data and safety monitoring board.

Study Design

A longitudinal prospective cohort study of 316 pregnant women at two sites, both academic tertiary care centers with Level VI neonatal intensive care units: OHSU and the UUHSC for three MRI studies at the following gestational ages: 12-16 weeks, 26-28 weeks, and 32-34 weeks (ClinicalTrials.gov: NCT02749851). The original prospective observational study design

had planned enrollment for 300 subjects to undergo the MRI studies in the aforementioned gestational windows. The rationale for the original exploratory study design was to facilitate characterization of T2* longitudinally during pregnancy and to minimize sensitivity to population variability in T2* values as a function of gestational age. A planned interim analysis in year 3 demonstrated tight correlation of T2* across study sites and within gestational age timepoints. As a result, the decision was made to open the gestational time windows for recruitment by +/- 8 weeks to facilitiate improved characterization of the evolution of placental T2* throughout pregnancy. The larger recruitment windows impacted the number of MRIs per study participant as some participants recruited later in gestation were not be able to complete additional MRI studies depending on the gestational age at enrollment. The decreased frequency of repeat MRI per study subject however did facilitate recruitment and enrollment of a larger study cohort than originally planned.

Participants were recruited from the OHSU and UUHSC clinics where written informed consent was obtained with IRB approval. Pregnant women were recruited based on inclusion criteria for two subject groups: a low-risk cohort not at increased risk for adverse obstetric outcome and a high-risk group at increased risk for adverse outcomes based on prior clinical history. A third group of pregnant tobacco smokers was originally planned as a separate cohort but recruitment was abandoned due to lack of success in identification and enrollment.

Inclusion criteria

Inclusion criteria for both groups included pregnancy (defined by positive pregnancy test and certain menstrual history, or early ultrasound) identified prior to 16 weeks gestation, maternal age over 18 years of age, and ability to give informed consent. The inclusion criteria for the low-risk cohort were all of the following: 1) no history of a second or third trimester pregnancy loss, 2) no history of fetal growth restriction, and 3) nonsmoker. The inclusion criteria for the high-risk group were one or more of the following: 1) history of pregnancy complicated by placental insufficiency in a previous singleton pregnancy defined by preeclampsia with severe features requiring preterm delivery, or preterm delivery due to placental insufficiency (fetal growth restriction, oligohydramnios, abnormal umbilical artery Doppler), or fetal growth restriction with neonatal weight < 10^{th} percentile delivered at term, or stillbirth attributed to placental cause, regardless of gestational age, 2) pregnancy at risk for placental insufficiency due to clinical comorbidities (i.e. chronic hypertension), or 3) history of spontaneous preterm birth < 34 weeks.

Exclusion criteria

Exclusion criteria were maternal intellectual disability or incarceration, pregnancy with major fetal anomalies known to be associated with abnormal fetal growth, active alcohol use during pregnancy, medical conditions requiring ongoing treatment during pregnancy including cancer, acute liver disease, chronic pulmonary disease requiring regular use of medication, history of claustrophobia, metal implants, or other contraindication for MRI, and increased risk of aneuploidy based on ultrasound findings and/or genetic testing.

Participant enrollment

Potential participants were identified through multiple modalities. The research team utilized social media, which entailed Facebook advertisements and promotions via institutional websites. The research teams also attended multiple pregnancy groups, such as prenatal group intake meetings and events for pregnant women, as well as a Portland-based website for new and expecting parents with resources and events. Potential research subjects were screened in the OHSU electronic medical record system, and Utah appointment logs through a waiver of authorization. Once participants were found via electronic medical records, they were approached at their next prenatal appointment or sent a MyChart message with pertinent research study information. When a potential subject reached out to the team via phone or email with interest, a phone screening was conducted. The phone screening reviewed basic eligibility inclusion and exclusion criteria, contact information, and additional preferences. If the subject was found to be eligible, they would be scheduled for a visit in accordance with the study protocol where they will start the visit with a detailed explanation of the study and followed with the signature of the informed consent. If not eligible for the study or no longer interested, they would be thanked for their time and interest.

Pregnancy outcome designation

Pregnancies were categorized postnatally into three groups: a) uncomplicated normal pregnancies (UN), b) primary adverse outcome pregnancies (PA), and c) secondary abnormal pregnancies (SA). Uncomplicated pregnancies were defined as those with term (37 weeks or beyond) delivery with birthweight between the 5^{th} and 95^{th} percentile, without gestational hypertensive disease, and not meeting any criteria for the primary adverse outcome or secondary abnormal outcome.

The primary adverse outcome group was defined using a composite including hypertensive disorders of pregnancy, with birthweight below the 5^{th} percentile by Oken (43), and stillbirth or fetal death. Hypertensive disorders of pregnancy included gestational hypertension,

preeclampsia without severe features, preeclampsia with severe features, Hemolysis, elevated liver enzymes, and low platelet count (HELLP) syndrome, and eclampsia. These were defined by ACOG criteria (52). Gestational hypertension was defined as systolic blood pressure of 140 mm Hg or more or a diastolic blood pressure of 90 mm Hg or more, or both, on two occasionas at least 4 hours apart at or beyond 20 weeks of gestation in someone without chronic hypertension. Preeclampsia was defined as elevated blood pressure (as in gestational hypertension) plus proteinuria (300mg or more in a 24 hour urine collection or urine protein/creatinine ratio of 0.3 or more) or presence of severe features without proteinuria. Severe features included systolic blood pressure of 160 mm Hg or more or diastolic blood pressure of 110 mm Hg or more on two occasions at least 4 hours apart, thrombocytopenia with platelet count < 100 x 10^9/L, liver enzymes more than twice the upper limit of normal, severe persistent right upper quadrant pain or epigastric pain, serum creatinine > 1.1 mg/dL, pulmonary edema, new headache unresponsive to medication, and/or visual disturbances. HELLP syndrome is defined by thromboycytopenia with platelet count < 100 x 10^9/L, liver enzymes more than twice the upper limit of normal, and evidence of hemolysis (LDH > 600 IU/L). Eclampsia was defined as seizure in absence of alternative etiology and with concomitant criteria for preeclampsia.

The secondary abnormal outcome group included pregnancies complicated by maternal chronic hypertension without superimposed preeclampsia, fetal genetic and/or anatomic anomalies; spontaneous preterm birth due to preterm labor, cervical insufficiency, and/or preterm premature rupture of the membranes (PPROM); placental abruption, chorioamnionitis, and/or birthweight greater than the 95th percentile by Oken (43). Our goal in creating this group was to capture pregnancy morbidity that is typically due to non-placental causes. Though morbidity can be significant in this group, our hypothesis was that our MRI protocol would not show strong association with these outcomes.

The primary adverse clinical composite outcome was developed pragmatically. Gestational hypertensive disease, preeclampsia, low birth weight, and fetal death/stillbirth are all linked to placental dysfunction (3, 50, 51). We acknowledge that this is not a pure phenotype, and there are multiple pathways to each of these outcomes, let alone the composite. However, this composite is clinically meaningful when attempting to capture morbidity and mortality due to placental insufficiency and there is significant overlap between the individual outcomes. Thus, in order to assess utility of MRI as a tool for either prediction or targeting of therapeutics, assessing these outcomes *in toto* is appropriate.

Adjudication of the primary adverse outcomes and secondary abnormal outcomes was performed independently by both of the Maternal-Fetal Medicine physicians at each site (OHSU: KJG, AEF; Utah: JMP, NRB). Any discordance between assessment of outcome was then discussed and reconciled prior to final determination. The authors determining the outcomes were blind to the MRI data and analysis. Similarly, MRI data acquisition and quality control was performed blind to pregnancy outcome group.

Magnetic Resonance Imaging

Maternal blood draws were performed prior to each scan and hemoglobin level measured using iStat (Abbott, Princeton, NJ) and/or fingerstick. Pulse oximetry (Zacurate 500BL) was used to determine maternal blood oxygen saturation level before each MRI study.

MRI in pregnant human volunteers was performed at up to three consecutive time points during pregnancy, ranging from 11 to 38 weeks gestation, on 3T Siemens Prisma scanner hardware using vendor spine and body array coils. Following localization of the uterus and placenta and acquisition of T2-HASTE anatomic imaging in three planes (axial, coronal, and sagittal), breath-hold multi-slice multi-echo gradient echo (MEGE) images were acquired in an axial orientation for T2* mapping, spanning the entire uterus with a spatial resolution of 1.75x1.75x3.5 mm, at six in-phase echo times (TE): 4.92/9.84/19.68/29.52/36.90/49.20 ms with a repetition time (TR) of 116 ms. Number of slices and in-plane coverage were adjusted as necessary to achieve complete coverage of the uterus and avoid image wrap. Breath hold duration was maintained below 10 seconds per acquisition to minimize patient discomfort. In OHSU studies, 3D variable flip angle T1 mapping was also performed with full placental coverage, using the Siemens MapIt protocol with flip angles of 3 and 15 degrees, including B1 correction (resolution 0.9x0.9x4 mm, TR=5.01, TE=2.23ms).

Image and data analysis

All post-processing, data modeling, and statistical analysis was performed in MATLAB (Mathworks, Natick MA) using standard library functions where available and custom in-house software otherwise. Quantitative T2* values were determined by weighted log-linear regression of MEGE signal magnitude measurements as described in detail in Schabel et al (34). Voxel-level uncertainty in estimated T2* values was computed from regression covariance matrices and propagation of errors analysis using measured magnitude noise levels in source MRI data. Three dimensional placental regions-of-interest (ROIs) were hand drawn on T2* maps, using co-registered T2-HASTE images as an anatomic reference when the placental-myometrial

and/or placental-fetal boundaries were indistinct. Slices with excessive image quality degradation arising from maternal and/or fetal motion were excluded from analysis. Readers were blinded to patient status and pregnancy outcome. Binary masks were derived from the placental ROIs, with T2* values of 250 ms or more being excluded from further analysis; such large values are associated with signal contamination by amniotic fluid. Placental volume was computed by summing the number of voxels in each slice of this binary mask multiplied by the per-voxel volume. Where slices were missing due to motion, volumes were estimated from adjacent slices using linear interpolation. In the OHSU cohort, median placental T1 was determined by spatially resampling measured T1 maps onto the T2* image volumes and applying placental ROIs.

Histogram analysis was used to compute median placental T2* for each study. Median relative fit uncertainty in T2* (the ratio of the model estimated sigma-T2* to estimated T2*) was computed as a measure of measurement quality. A heuristic quality statistic was determined by computing the fraction of placental voxels for which the relative fit uncertainty was <= 0.25. Sensitivity of the data analysis pipeline to data quality was evaluated by re-running the entire statistical post-processing pipeline for both the entire set of studies and for a reduced set where studies with either median relative uncertainty in the highest 10% or heuristic quality in the lowest 10% were excluded. Potential bias stemming from variation in the number of scans per patient ranging from one to three was considered by re-running the post-processing pipeline with scan weight distributed evenly per patient, rather than per scan.

Trends in maternal SpO2, maternal hemoglobin concentration, placental volume, and placental T1 across gestational age were found to be well fit with a linear model. Gestational trends in T2* were modeled sequentially with linear and quadratic polynomials as well as with a logistic function ($T_2^*(t) = p_1/(1 + \exp(p_2(t - p_3))) + p_4$), which was chosen based on the sigmoidal behavior observed in median T2* curves in normal pregnancies. Regression modeling used **`polyfit`** for polynomial fitting and **`nlinfit`** for nonlinear model fitting to T2* data, with regressions weighted by measurement uncertainties. The Bayes Information Criterion (BIC) was used to account for different numbers of free parameters for model selection. Based on the BIC results, the sigmoid function was determined to have the best fit to measured T2* data. Intra-individual time derivatives in T2* across gestational age were approximated as pairwise centered finite differences from measurements acquired at sequential gestational time points: $(\Delta T_2^*/\Delta t)((t_1 + t_2)/2) = (T_2^*(t_2) - T_2^*(t_1))/(t_2 - t_1)$. The resulting data were fit with the time derivative of the logistic function: $(\Delta T_2^*/\Delta t)(t) = -p_1 p_2 \exp\,(p_2(t - p_3))/(1 + \exp(p_2(t - p_3)))^2$.

Fit covariance matrices were used to compute model parameter uncertainties as well as 95% confidence and prediction intervals for all regressions. Model regressions were considered to be significantly different where their 95% confidence intervals were non-overlapping. In addition to the three primary study groups (UN pregnancies, SA pregnancies, and PA pregnancies), differences between UN at the two study sites were compared, along with differences based on fetal sex, maternal age, and maternal BMI.

A model describing the observed inter-site T2* differences across gestation between OHSU and Utah sub-populations was developed starting from the assumption that these differences arise from corresponding site-dependent differences in maternal hemoglobin and SpO2 levels, along with a maternal placental blood volume fraction that evolves through pregnancy. The resultant shift is most easily described in terms of differences in the transverse relaxation rate, defined as $R_2^* = 1/T_2^*$, between site A (OHSU) and site B (Utah) using the known transverse relaxivity of deoxyhemoglobin (r_2^*=20.2/mmol/s) and blood deoxyhemoglobin concentrations computed from measured maternal SpO2, along with the maternal placental blood volume fraction (v_{mpb}):

$$\Delta R_2^*(t) = r_2^* \left([Hb(t)]_A \left(100 - \left(S_p O_2(t)\right)_A\right) - [Hb(t)]_B \left(100 - \left(S_p O_2(t)\right)_B\right)\right) v_{mpb}(t).$$

Combining this expression with the modeled dependence of maternal SpO2 and hemoglobin levels for the two sites allows us to solve for the gestation-dependent value of $v_{mpb}(t)$ that corresponds to observed differences in placental T2*. This parameter is a volume fraction that should correspond approximately to *in vivo* intervillous volume (55), and is physically-constrained to lie in the closed interval [0,1].

Z-scores were computed for all placental T2* measurements using the model regression and prediction intervals for UN pregnancies, and T2* percentiles were calculated from the cumulative distribution function (CDF) of the corresponding normal distribution. Receiver operating characteristic (ROC) curves were then generated from the T2* percentiles for all individual studies in UN vs. PA pregnancies (SA pregnancies were omitted from this analysis). Studies were also grouped into three gestational time windows: early gestation (10-20 weeks), mid-gestation (20-30 weeks), and late gestation (30-40 weeks) in order to assess the performance of this metric across gestation, and ROCs were separately computed for OHSU and Utah data to compare the site-specific performance.

Statistics

All p-values for continuous variables presented in this manuscript were computed using a two-tailed Kolmogorov-Smirnov test. The chi-square proportion test was used to compute p-values of binary variables. Significance of differences in model regressions was assessed using the presence or absence of overlapping 95% confidence intervals.

Tables

Table 1: Demographic data from the study populations at OHSU and Utah.

Table 2: Breakdown of prenatal conditions in the primary adverse outcome group for entire PA population and by site.

Table 3: Regression models, best fit parameter values and estimated parameter uncertainties, and RMS fit residual values for model fits of gestational trends in T2*, $\Delta T2^*/\Delta GW$, maternal hemoglobin, maternal blood oxygen saturation, *in vivo* placental volume, and T1. Fits are presented for the aggregate data set along with separate regressions to the OHSU and Utah subpopulations for normal pregnancies.

Acknowledgements

This work was supported by: NICHD Human Placenta Project U01 HD 087182 (Frias) and R01 HD 086331 (Frias): NIH S10OD021701 for the 3T Siemens Prisma MRI instrument, housed in OHSU's Advanced Imaging Research Center: NIH S10OD018224 for the High Performance Computing Cluster, housed in OHSU's Advanced Imaging Research Center: the Oregon Clinical & Translational Research Institute grant which supported the use of REDCap (Research Electronic Data Capture) for data abstraction (CTSA Award No.: UL1TR002369).

Author contributions.

MCS, VHJR, CDK, RMS, AEF: Conceived and designed study. AEF, VHJR, MR, KJG, MWV, KS: Coordinated and facilitated subject recruitment, enrollment and participation in the study. MCS, VHJR, KJG, AEF, NRB, JMP, CDK, BP, MWV, RMS: Reviewed the data and aided in experimental design. MCS, VHJR, KJG, AEF: drafted the manuscript. All authors reviewed the manuscript. MCS: Supervised and acquired MRI data, developed software for MRI data post-processing and analysis, performed MRI data analysis. ADS, AMW, JOL: Assisted with MRI data analysis. MR, JEG, KS, KH: Assisted and facilitated RedCap data entry. MCS, BP: Designed and performed statistical analysis.

Figure legends

Figure 1: Enrollment flow chart.

A flow chart detailing numbers of prospective patients screened, consented, and enrolled at both study sites, along with numbers of completed MRI studies meeting quality criteria for inclusion in data analysis presented here.

Figure 2: Comparison of anatomic imaging (T2-weighted HASTE, left column) and placental T2* mapping (right column) in a uncomplicated normal pregnancy at 232 days gestation (top row, panels A & B) with those from a primary adverse pregnancy at 235 days gestation presenting with severe preeclampsia (bottom row, panels C & D). The placenta is indicated by the dashed blue outlines overlaid on the T2* maps.

Figure 3: Gestational dependence of placental T2* values.

Median T2* values for each completed study, computed over the entire placenta, are plotted as a function of gestational age at time of imaging in the three panels in the left column (panels A, B, C), while corresponding rates of change in placental T2* between repeated imaging time points within the same individual are plotted as a function of gestational age in the right column (panels D, E, F). The upper row plots these quantities for normal pregnancies, the middle row for abnormal (green) and adverse (red) pregnancies, and the bottom row for normal pregnancies stratified by site (OHSU in blue, Utah in red). In all graphs, model regression curves (using the functions defined in Table 2) are indicated by the thick solid lines, the 95% confidence intervals by the dashed lines, and the 95% prediction intervals by the dot-dashed lines. The best fit and 95% CI curves from the plots in the upper row are shown in gray in the middle and bottom rows for reference.

Figure 4: Histograms of T2* z-scores in normal, abnormal, and adverse pregnancies.

Z-score histograms shown are computed using prediction intervals for sigmoid model regression to T2* measurements in UN pregnancies, applied to individual studies in UN (blue), PA (red), and SA (green) pregnancies.

Figure 5: Bar chart of distribution of measured T2* percentiles for uncomplicated normal, primary adverse, and secondary abnormal pregnancies.

Figure 6: Receiver operator characteristic (ROC) curves for T2* measurements in pregnancies with our primary adverse outcome relative to uncomplicated normal pregnancies.

The points where Youden's J is maximized are indicated by the stars. Area under the curve (AUC), J_{max}, and the corresponding optimal cutoff threshold in T2* percentile relative to UN (C_{opt}) are given in the figure legend for each panel.

Table 1: Demographic data for uncomplicated (UN), primary adverse (PA), and secondary abnormal (SA) groups, for entire study population and separated by study site.

	UN			PA			SA		
	All	OHSU	Utah	All	OHSU	Utah	All	OHSU	Utah
Maternal age at conception	31.2 (4.6)	31.8 (5.1)	30.4 (4.0)	31.7 (5.1)	32.2 (5.3)	31.0 (4.9)	31.0 (5.4)	30.9 (5.7)	31.4 (4.7)
Race									
White	175 (81.4%)	97 (79.5%)	78 (83.9%)	55 (75.3%)	29 (69.0%)	26 (83.9%)	42 (73.7%)	27 (69.2%)	15 (83.3%)
African Descent	9 (4.2%)	9 (7.4%)	0 (0.0%)	1 (1.4%)	1 (2.4%)	0 (0.0%)	2 (3.5%)	1 (2.6%)	1 (5.6%)
Native American	5 (2.3%)	3 (2.5%)	2 (2.2%)	0 (0.0%)	0 (0.0%)	0 (0.0%)	3 (5.3%)	2 (5.1%)	1 (5.6%)
Asian Indian	4 (1.9%)	3 (2.5%)	1 (1.1%)	1 (1.4%)	0 (0.0%)	1 (3.2%)	0 (0.0%)	0 (0.0%)	0 (0.0%)
Other Asian	10 (4.7%)	6 (4.9%)	4 (4.3%)	6 (8.2%)	4 (9.5%)	2 (6.5%)	2 (3.5%)	2 (5.1%)	0 (0.0%)
Native Hawaiian	0 (0.0%)	0 (0.0%)	0 (0.0%)	0 (0.0%)	0 (0.0%)	0 (0.0%)	1 (1.8%)	1 (2.6%)	0 (0.0%)
Pacific Islander	0 (0.0%)	0 (0.0%)	0 (0.0%)	1 (1.4%)	0 (0.0%)	1 (3.2%)	1 (1.8%)	1 (2.6%)	0 (0.0%)
Other	1 (0.5%)	1 (0.8%)	0 (0.0%)	0 (0.0%)	0 (0.0%)	0 (0.0%)	0 (0.0%)	0 (0.0%)	0 (0.0%)
Unknown	1 (0.5%)	1 (0.8%)	0 (0.0%)	0 (0.0%)	0 (0.0%)	0 (0.0%)	0 (0.0%)	0 (0.0%)	0 (0.0%)
Hispanic	10 (4.7%)	2 (1.6%)	8 (8.6%)	9 (12.3%)	8 (19.0%)	1 (3.2%)	6 (10.5%)	5 (12.8%)	1 (5.6%)
Pre-pregnancy BMI	24.4 (4.4)	24.7 (4.8)	24.0 (3.9)	26.3 (5.9)	27.4 (6.5)	24.8 (4.8)	36.7 (5.8)	27.2 (6.2)	25.4 (4.6)

634

Table 2: Breakdown of prenatal conditions in the primary adverse outcome group for entire PA population and by site.

Outcome	Total N=74	OHSU N=39	Utah N=31	p-value
PIH	59 (84.3%)	34 (87.2%)	25 (80.6%)	0.68
Gestational HTN	22 (31.4%)	13 (33.3%)	9 (29.0%)	0.90
Pre-e w/o sev	9 (12.8%)	3 (7.7%)	6 (19.4%)	0.28
Pre-e w/sev	28 (40.0%)	18 (46.2%)	10 (32.2%)	0.35
SGA	14 (20.0%)	9 (23.1%)	4 (16.1%)	0.44
Stillbirth or fetal loss	4 (5.7%)	1 (2.6%)	3 (9.7%)	0.45
Placental abruption	2 (2.8%)	0 (0.0%)	2 (6.4%)	0.38
Both PIH + SGA	5 (7.1%)	3 (7.7%)	2 (6.4%)	0.79
Preterm birth (<37w)	31 (35.7%)	13 (33.3%)	12 (38.7%)	0.83

635

	p_1	p_2	p_3	p_4	RMS_{fit}
Median T2* (ms)	$T_2^*(t) = p_1/(1+\exp(p_2(t-p_3))) + p_4$				
UN pregnancies	-59.2 (+/-6.5)	-0.24 (+/-0.04)	29.3 (+/-0.8)	84.6 (+/-1.3)	+/-9.6 ms
OHSU only	-59.3 (+/-7.6)	-0.26 (+/-0.05)	29.4 (+/-0.9)	86.3 (+/-1.5)	+/-9.5 ms
Utah only	-62.8 (+/-13.9)	-0.20 (+/-0.06)	29.5 (+/-1.8)	83.6 (+/-2.8)	+/-9.2 ms
SA pregnancies	-53.7 (+/-11.3)	-0.28 (+/-0.11)	26.8 (+/-1.3)	85.4 (+/-4.0)	+/-12.5 ms
PA pregnancies	-57.6 (+/-22.9)	-0.19 (+/-0.11)	25.2 (+/-2.0)	82.9 (+/-10.7)	+/-13.8 ms
ΔT2*/ΔGW (ms/week)	$\Delta T_2^*/\Delta t(t) = -p_1 p_2 \exp(p_2(t-p_3))/(1+\exp(p_2(t-p_3)))^2$				
UN pregnancies	-64.9 (+/-4.2)	-0.20 (+/-0.01)	30.1 (+/-0.6)		+/-1.2 ms/wk
OHSU only	-75.5 (+/-9.5)	-0.19 (+/-0.02)	31.3 (+/-1.1)		+/-1.0 ms/wk
Utah only	-60.2 (+/-5.0)	-0.20 (+/-0.02)	29.6 (+/-0.7)		+/-1.1 ms/wk
SA pregnancies	-79.0 (+/-22.0)	-0.16 (+/-0.04)	30.7 (+/-2.6)		+/-1.4 ms/wk
PA pregnancies	-5574.6 (+/-1e6)	-0.02 (+/-0.24)	225.9 (+/-2e5)		+/-1.4 ms/wk
[Hb] (mg/dl)	$[Hb](t) = p_1 + p_2 t$				
UN pregnancies	13.27 (+/-0.15)	-0.046 (+/-0.006)			+/-1.02 mg/dl
OHSU only	12.86 (+/-0.17)	-0.047 (+/-0.007)			+/-0.86 mg/dl
Utah only	13.78 (+/-0.21)	-0.042 (+/-0.008)			+/-0.90 mg/dl
SA pregnancies	12.65 (+/-0.32)	-0.018 (+/-0.013)			+/-0.92 mg/dl
PA pregnancies	13.46 (+/-0.31)	-0.039 (+/-0.012)			+/-1.04 mg/dl
SpO2 (%)	$SpO_2(t) = p_1 + p_2 t$				
UN pregnancies	97.05 (+/-0.57)	0.003 (+/-0.021)			+/-2.4%
OHSU only	98.37 (+/-0.38)	-0.010 (+/-0.014)			+/-1.2%
Utah only	95.24 (+/-1.03)	0.031 (+/-0.037)			+/-3.0%
SA pregnancies	98.54 (+/-0.65)	-0.043 (+/-0.025)			+/-1.4%
PA pregnancies	95.99 (+/-1.16)	0.052 (+/-0.044)			+/-3.1%
Placental volume (cm^3)	$V(t) = p_1 + p_2 t$				
UN pregnancies	-372.4 (+/-17.6)	32.2 (+/-0.68)			+/-122 cm^3
OHSU only	-377.0 (+/-25.9)	32.4 (+/-0.99)			+/-130 cm^3
Utah only	-367.7 (+/-23.6)	32.1 (+/-0.91)			+/-113 cm^3
SA pregnancies	-383.0 (+/-53.5)	33.1 (+/-2.18)			+/-158 cm^3
PA pregnancies	-360.5 (+/-35.7)	30.0 (+/-1.40)			+/-132 cm^3
Median T1 (ms)	$T_1(t) = p_1 + p_2 t$				
UN pregnancies	---	---			
OHSU only	2513.3 (+/-49.3)	-26.9 (+/-1.88)			+/-208 ms
Utah only	---	---			
SA pregnancies	2555.7 (+/-83.0)	-26.5 (+/-3.37)			+/-158 ms
PA pregnancies	2591.2 (+/-102.0)	-31.2 (+/-3.87)			+/-246 ms

Table 3. Model fit functions and parameters. Functional forms used for model regression to measured data are indicated for the various data sets described in the text are indicated, along with best-fit model parameter values and parameter uncertainties, and RMS values for model fit residuals (rightmost column). All times (t) are in gestational weeks.

References 1. Hennington BS, Alexander BT. Linking intrauterine growth restriction and blood pressure: insight into the human origins of cardiovascular disease. Circulation. 2013;128(20):2179-80.
2. Jaddoe VW, de Jonge LL, Hofman A, Franco OH, Steegers EA, Gaillard R. First trimester fetal growth restriction and cardiovascular risk factors in school age children: population based cohort study. BMJ. 2014;348:g14.
3. Kovo M, Schreiber L, Bar J. Placental vascular pathology as a mechanism of disease in pregnancy complications. Thromb Res. 2013;131 Suppl 1:S18-21.
4. Kovo M, Schreiber L, Ben-Haroush A, Gold E, Golan A, Bar J. The placental component in early-onset and late-onset preeclampsia in relation to fetal growth restriction. Prenat Diagn. 2012;32(7):632-7.
5. Paranjothy S, Dunstan F, Watkins WJ, Hyatt M, Demmler JC, Lyons RA, et al. Gestational age, birth weight, and risk of respiratory hospital admission in childhood. Pediatrics. 2013;132(6):e1562-9.
6. Sehgal A, Doctor T, Menahem S. Cardiac function and arterial biophysical properties in small for gestational age infants: postnatal manifestations of fetal programming. J Pediatr. 2013;163(5):1296-300.
7. Walker CK, Krakowiak P, Baker A, Hansen RL, Ozonoff S, Hertz-Picciotto I. Preeclampsia, placental insufficiency, and autism spectrum disorder or developmental delay. JAMA Pediatr. 2015;169(2):154-62.
8. Bar J, Schreiber L, Ben-Haroush A, Ahmed H, Golan A, Kovo M. The placental vascular component in early and late intrauterine fetal death. Thromb Res. 2012;130(6):901-5.
9. Cruz-Lemini M, Crispi F, Van Mieghem T, Pedraza D, Cruz-Martinez R, Acosta-Rojas R, et al. Risk of perinatal death in early-onset intrauterine growth restriction according to gestational age and cardiovascular Doppler indices: a multicenter study. Fetal Diagn Ther. 2012;32(1-2):116-22.
10. Dicke JM, Huettner P, Yan S, Odibo A, Kraus FT. Umbilical artery Doppler indices in small for gestational age fetuses: correlation with adverse outcomes and placental abnormalities. J Ultrasound Med. 2009;28(12):1603-10.
11. Kidron D, Bernheim J, Aviram R. Placental findings contributing to fetal death, a study of 120 stillbirths between 23 and 40 weeks gestation. Placenta. 2009;30(8):700-4.
12. Pare E, Parry S, McElrath TF, Pucci D, Newton A, Lim KH. Clinical risk factors for preeclampsia in the 21st century. Obstet Gynecol. 2014;124(4):763-70.
13. Roberts DJ, Post MD. The placenta in pre-eclampsia and intrauterine growth restriction. J Clin Pathol. 2008;61(12):1254-60.
14. Salafia CM, Vintzileos AM, Silberman L, Bantham KF, Vogel CA. Placental pathology of idiopathic intrauterine growth retardation at term. Am J Perinatol. 1992;9(3):179-84.
15. Salafia CM, Vogel CA, Bantham KF, Vintzileos AM, Pezzullo J, Silberman L. Preterm delivery: correlations of fetal growth and placental pathology. Am J Perinatol. 1992;9(3):190-3.
16. Sibai B, Dekker G, Kupferminc M. Pre-eclampsia. Lancet. 2005;365(9461):785-99.
17. Stillbirth Collaborative Research Network Writing G. Association between stillbirth and risk factors known at pregnancy confirmation. JAMA. 2011;306(22):2469-79.
18. Bell AW, Hay WW, Jr., Ehrhardt RA. Placental transport of nutrients and its implications for fetal growth. J Reprod Fertil Suppl. 1999;54:401-10.
19. Gude NM, Roberts CT, Kalionis B, King RG. Growth and function of the normal human placenta. Thromb Res. 2004;114(5-6):397-407.
20. Murphy VE, Smith R, Giles WB, Clifton VL. Endocrine regulation of human fetal growth: the role of the mother, placenta, and fetus. Endocr Rev. 2006;27(2):141-69.
21. Ozkaya U, Ozkan S, Ozeren S, Corakci A. Doppler examination of uteroplacental circulation in early pregnancy: can it predict adverse outcome? J Clin Ultrasound. 2007;35(7):382-6.

22. Poon LC, Lesmes C, Gallo DM, Akolekar R, Nicolaides KH. Prediction of small-for-gestational-age neonates: screening by biophysical and biochemical markers at 19-24 weeks. Ultrasound Obstet Gynecol. 2015;46(4):437-45.
23. Su EJ. Role of the fetoplacental endothelium in fetal growth restriction with abnormal umbilical artery Doppler velocimetry. Am J Obstet Gynecol. 2015;213(4 Suppl):S123-30.
24. Verlohren S, Melchiorre K, Khalil A, Thilaganathan B. Uterine artery Doppler, birth weight and timing of onset of pre-eclampsia: providing insights into the dual etiology of late-onset pre-eclampsia. Ultrasound Obstet Gynecol. 2014;44(3):293-8.
25. Zhong Y, Tuuli M, Odibo AO. First-trimester assessment of placenta function and the prediction of preeclampsia and intrauterine growth restriction. Prenat Diagn. 2010;30(4):293-308.
26. Tuuli MG, Odibo AO. The role of serum markers and uterine artery Doppler in identifying at-risk pregnancies. Clin Perinatol. 2011;38(1):1-19, v.
27. Mitra SC, Seshan SV, Riachi LE. Placental vessel morphometry in growth retardation and increased resistance of the umbilical artery Doppler flow. J Matern Fetal Med. 2000;9(5):282-6.
28. O'Dwyer V, Burke G, Unterscheider J, Daly S, Geary MP, Kennelly MM, et al. Defining the residual risk of adverse perinatal outcome in growth-restricted fetuses with normal umbilical artery blood flow. Am J Obstet Gynecol. 2014;211(4):420 e1-5.
29. Unterscheider J, Daly S, Geary MP, Kennelly MM, McAuliffe FM, O'Donoghue K, et al. Optimizing the definition of intrauterine growth restriction: the multicenter prospective PORTO Study. Am J Obstet Gynecol. 2013;208(4):290 e1-6.
30. Guttmacher AE, Maddox YT, Spong CY. The Human Placenta Project: placental structure, development, and function in real time. Placenta. 2014;35(5):303-4.
31. Sorensen A, Peters D, Frund E, Lingman G, Christiansen O, Uldbjerg N. Changes in human placental oxygenation during maternal hyperoxia estimated by blood oxygen level-dependent magnetic resonance imaging (BOLD MRI). Ultrasound Obstet Gynecol. 2013;42(3):310-4.
32. Ogawa S, Lee TM, Kay AR, Tank DW. Brain magnetic resonance imaging with contrast dependent on blood oxygenation. Proc Natl Acad Sci U S A. 1990;87(24):9868-72.
33. Frias AE, Schabel MC, Roberts VH, Tudorica A, Grigsby PL, Oh KY, et al. Using dynamic contrast-enhanced MRI to quantitatively characterize maternal vascular organization in the primate placenta. Magn Reson Med. 2015;73(4):1570-8.
34. Schabel MC, Roberts VHJ, Lo JO, Platt S, Grant KA, Frias AE, et al. Functional imaging of the nonhuman primate Placenta with endogenous blood oxygen level-dependent contrast. Magn Reson Med. 2016;76(5):1551-62.
35. Hirsch AJ, Roberts VHJ, Grigsby PL, Haese N, Schabel MC, Wang X, et al. Zika virus infection in pregnant rhesus macaques causes placental dysfunction and immunopathology. Nat Commun. 2018;9(1):263.
36. Lo JO, Roberts VHJ, Schabel MC, Wang X, Morgan TK, Liu Z, et al. Novel Detection of Placental Insufficiency by Magnetic Resonance Imaging in the Nonhuman Primate. Reprod Sci. 2018;25(1):64-73.
37. Lo JO, Schabel MC, Roberts VH, Wang X, Lewandowski KS, Grant KA, et al. First trimester alcohol exposure alters placental perfusion and fetal oxygen availability affecting fetal growth and development in a non-human primate model. Am J Obstet Gynecol. 2017;216(3):302 e1- e8.
38. Anderson KB, Andersen AS, Hansen DN, Sinding M, Peters DA, Frokjaer JB, et al. Placental transverse relaxation time (T2) estimated by MRI: Normal values and the correlation with birthweight. Acta Obstet Gynecol Scand. 2020.
39. Hutter J, Slator PJ, Jackson L, Gomes ADS, Ho A, Story L, et al. Multi-modal functional MRI to explore placental function over gestation. Magn Reson Med. 2019;81(2):1191-204.
40. Melbourne A, Aughwane R, Sokolska M, Owen D, Kendall G, Flouri D, et al. Separating fetal and maternal placenta circulations using multiparametric MRI. Magn Reson Med. 2019;81(1):350-61.

731 41. Nye GA, Ingram E, Johnstone ED, Jensen OE, Schneider H, Lewis RM, et al. Human placental
732 oxygenation in late gestation: experimental and theoretical approaches. J Physiol. 2018;596(23):5523-
733 34.
734 42. Sinding M, Peters DA, Poulsen SS, Frokjaer JB, Christiansen OB, Petersen A, et al. Placental
735 baseline conditions modulate the hyperoxic BOLD-MRI response. Placenta. 2018;61:17-23.
736 43. Schabel MC, Roberts VHJ, Rincon DM, Gaffney JE, Lo JO, Gibbins KJ, et al. A Longitudinal
737 Multisite Study of Endogenous BOLD MRI In Human Pregnancies. Magnetic Resonance in Medicine.
738 2019:1075.
739 44. You W, Andescavage NN, Kapse K, Donofrio MT, Jacobs M, Limperopoulos C. Hemodynamic
740 Responses of the Placenta and Brain to Maternal Hyperoxia in Fetuses with Congenital Heart Disease by
741 Using Blood Oxygen-Level Dependent MRI. Radiology. 2020;294(1):141-8.
742 45. Oken E, Kleinman KP, Rich-Edwards J, Gillman MW. A nearly continuous measure of birth weight
743 for gestational age using a United States national reference. BMC Pediatr. 2003;3:6.
744 46. Leon RL, Li KT, Brown BP. A retrospective segmentation analysis of placental volume by
745 magnetic resonance imaging from first trimester to term gestation. Pediatr Radiol. 2018;48(13):1936-44.
746 47. Oh KY, Roberts VH, Schabel MC, Grove KL, Woods M, Frias AE. Gadolinium Chelate Contrast
747 Material in Pregnancy: Fetal Biodistribution in the Nonhuman Primate. Radiology. 2015;276(1):110-8.
748 48. Prola-Netto J, Woods M, Roberts VHJ, Sullivan EL, Miller CA, Frias AE, et al. Gadolinium Chelate
749 Safety in Pregnancy: Barely Detectable Gadolinium Levels in the Juvenile Nonhuman Primate after in
750 Utero Exposure. Radiology. 2018;286(1):122-8.
751 49. Gestational Hypertension and Preeclampsia: ACOG Practice Bulletin, Number 222. Obstet
752 Gynecol. 2020;135(6):e237-e60.
753 50. Gibbins KJ, Pinar H, Reddy UM, Saade GR, Goldenberg RL, Dudley DJ, et al. Findings in Stillbirths
754 Associated with Placental Disease. Am J Perinatol. 2020;37(7):708-15.
755 51. Spinillo A, Gardella B, Bariselli S, Alfei A, Silini E, Dal Bello B. Placental histopathological
756 correlates of umbilical artery Doppler velocimetry in pregnancies complicated by fetal growth
757 restriction. Prenat Diagn. 2012;32(13):1263-72.
758 52. Mayhew TM. Patterns of villous and intervillous space growth in human placentas from normal
759 and abnormal pregnancies. Eur J Obstet Gynecol Reprod Biol. 1996;68(1-2):75-82.
760

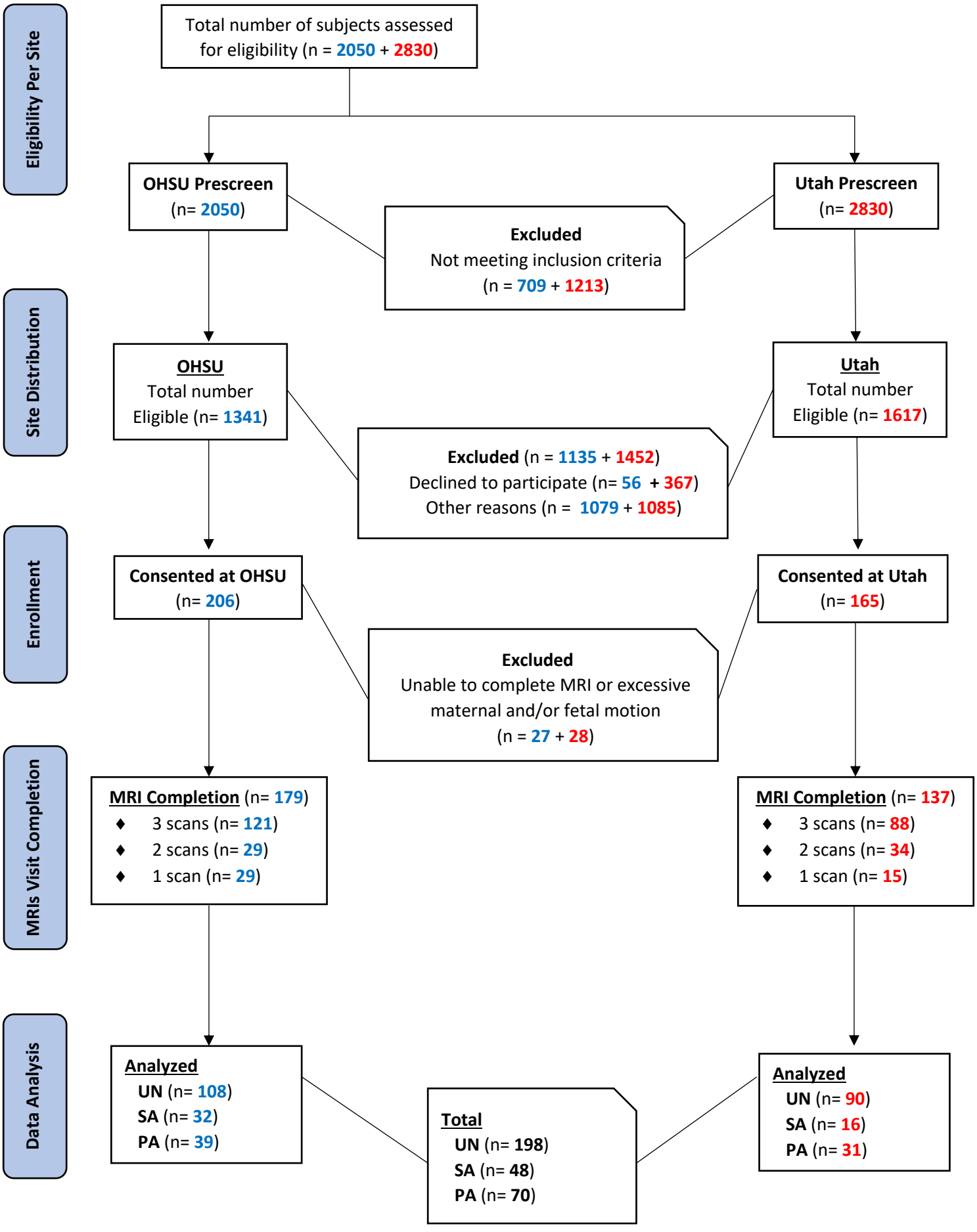
Eligibility Per Site
Total number of subjects assessed for eligibility (n = 2050 + 2830)
OHSU Prescreen (n= 2050)
Utah Prescreen (n= 2830)
Excluded
Not meeting inclusion criteria
(n = 709 + 1213)
Site Distribution
OHSU
Total number
Eligible (n= 1341)
Utah
Total number
Eligible (n= 1617)
Excluded (n = 1135 + 1452)
Declined to participate (n= 56 + 367)
Other reasons (n = 1079 + 1085)
Enrollment
Consented at OHSU (n= 206)
Consented at Utah (n= 165)
Excluded
Unable to complete MRI or excessive maternal and/or fetal motion
(n = 27 + 28)
MRIs Visit Completion
MRI Completion (n= 179)
3 scans (n= 121)
2 scans (n= 29)
1 scan (n= 29)
MRI Completion (n= 137)
3 scans (n= 88)
2 scans (n= 34)
1 scan (n= 15)
Data Analysis
Analyzed
UN (n= 108)
SA (n= 32)
PA (n= 39)
Total
UN (n= 198)
SA (n= 48)
PA (n= 70)
Analyzed
UN (n= 90)
SA (n= 16)
PA (n= 31)

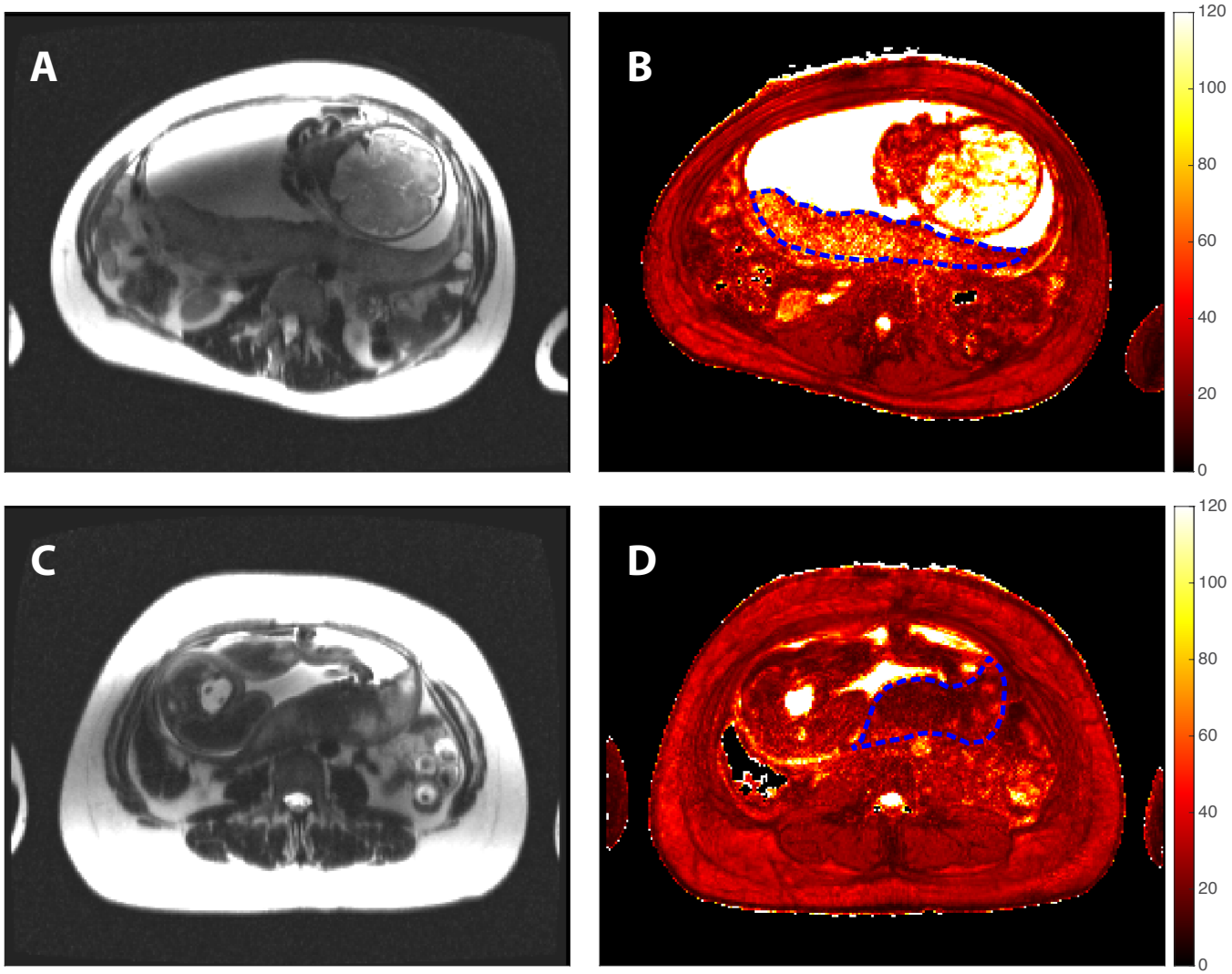

Figure 2

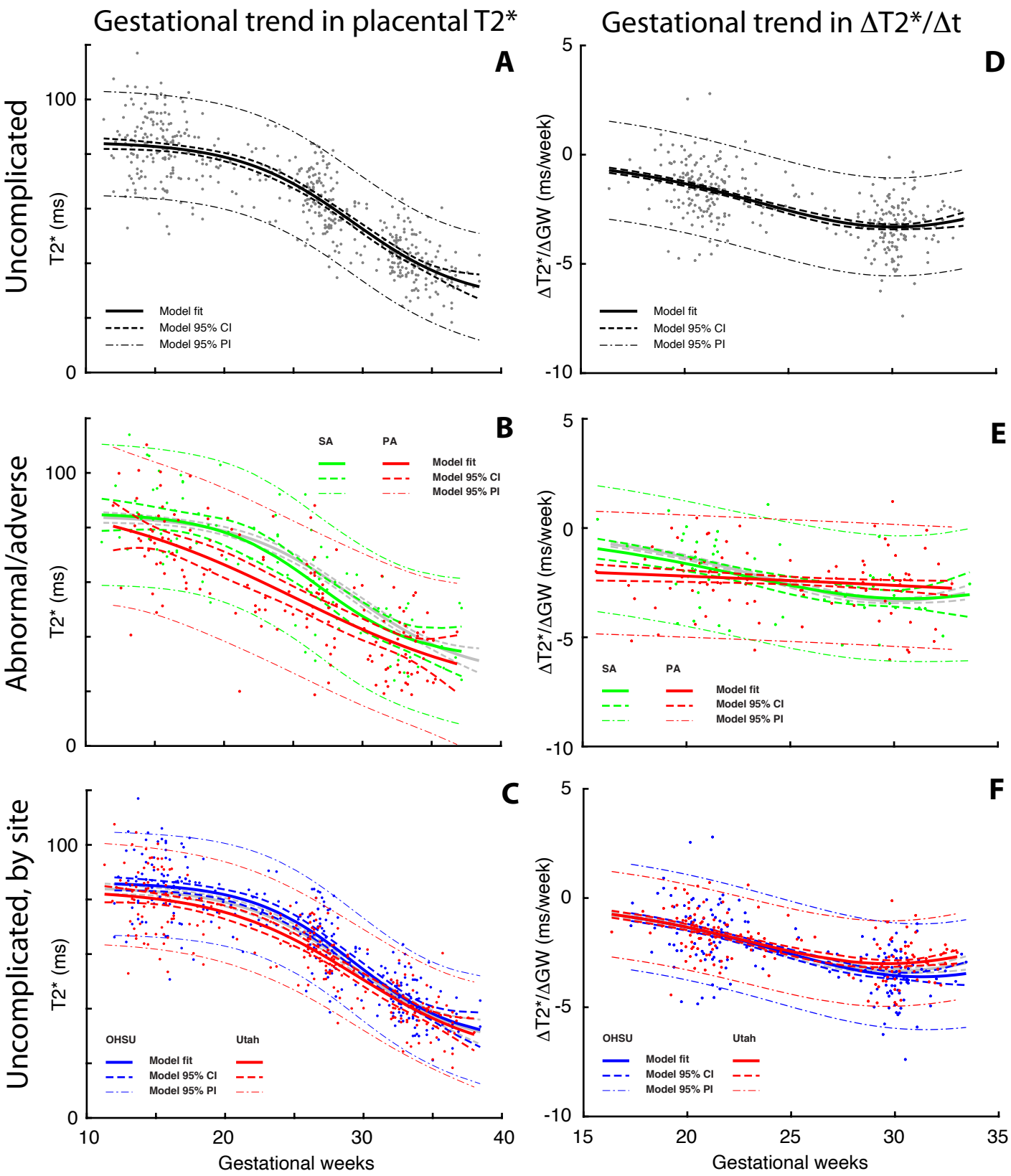
Gestational trend in placental T2*
Gestational trend in ΔT2*/Δt
Uncomplicated
Abnormal/adverse
Uncomplicated, by site
A
B
C
D
E
F
T2* (ms)
ΔT2*/ΔGW (ms/week)
Gestational weeks
Model fit
Model 95% CI
Model 95% PI
SA
PA
OHSU
Utah

Figure 3

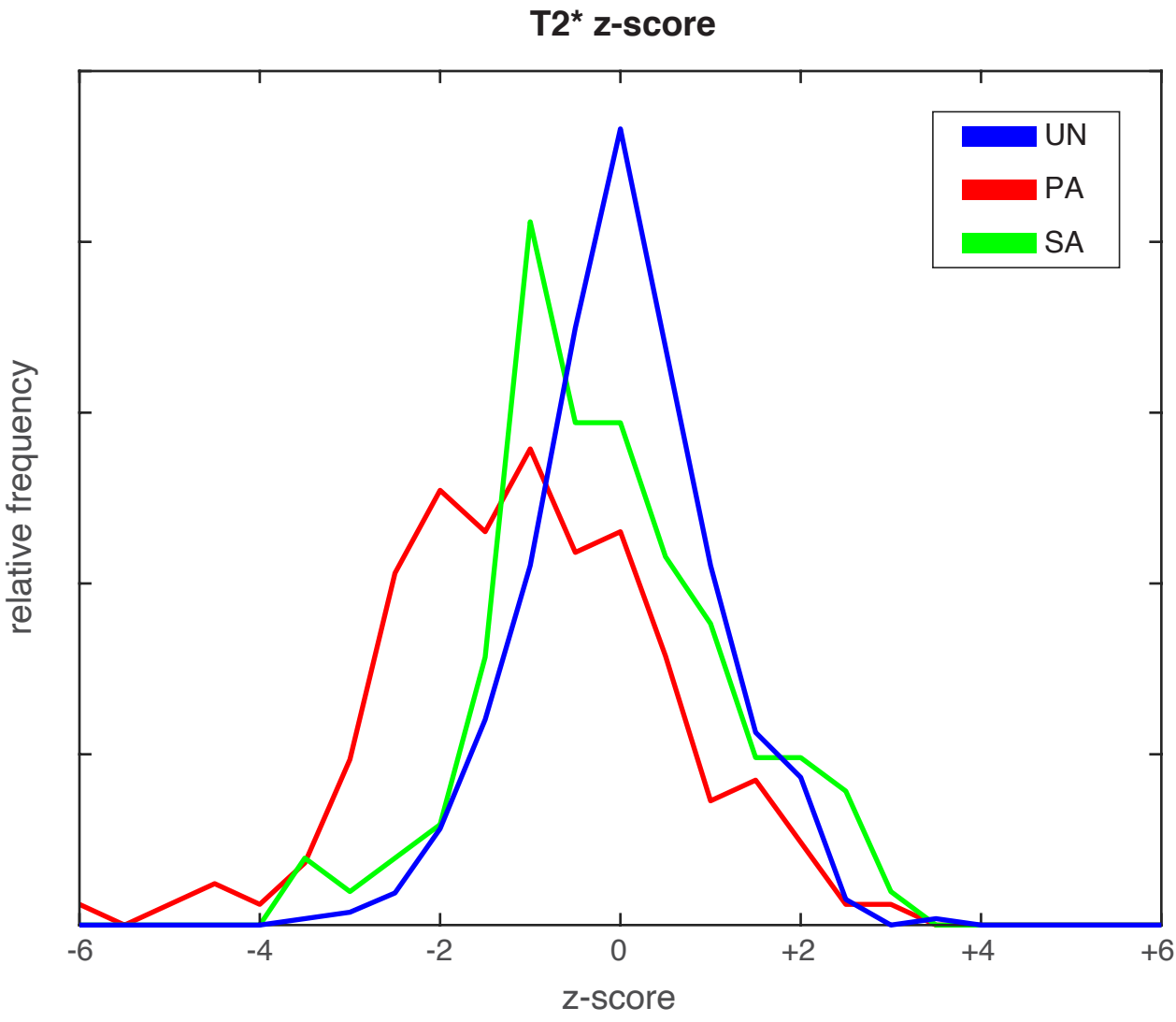

Figure 4

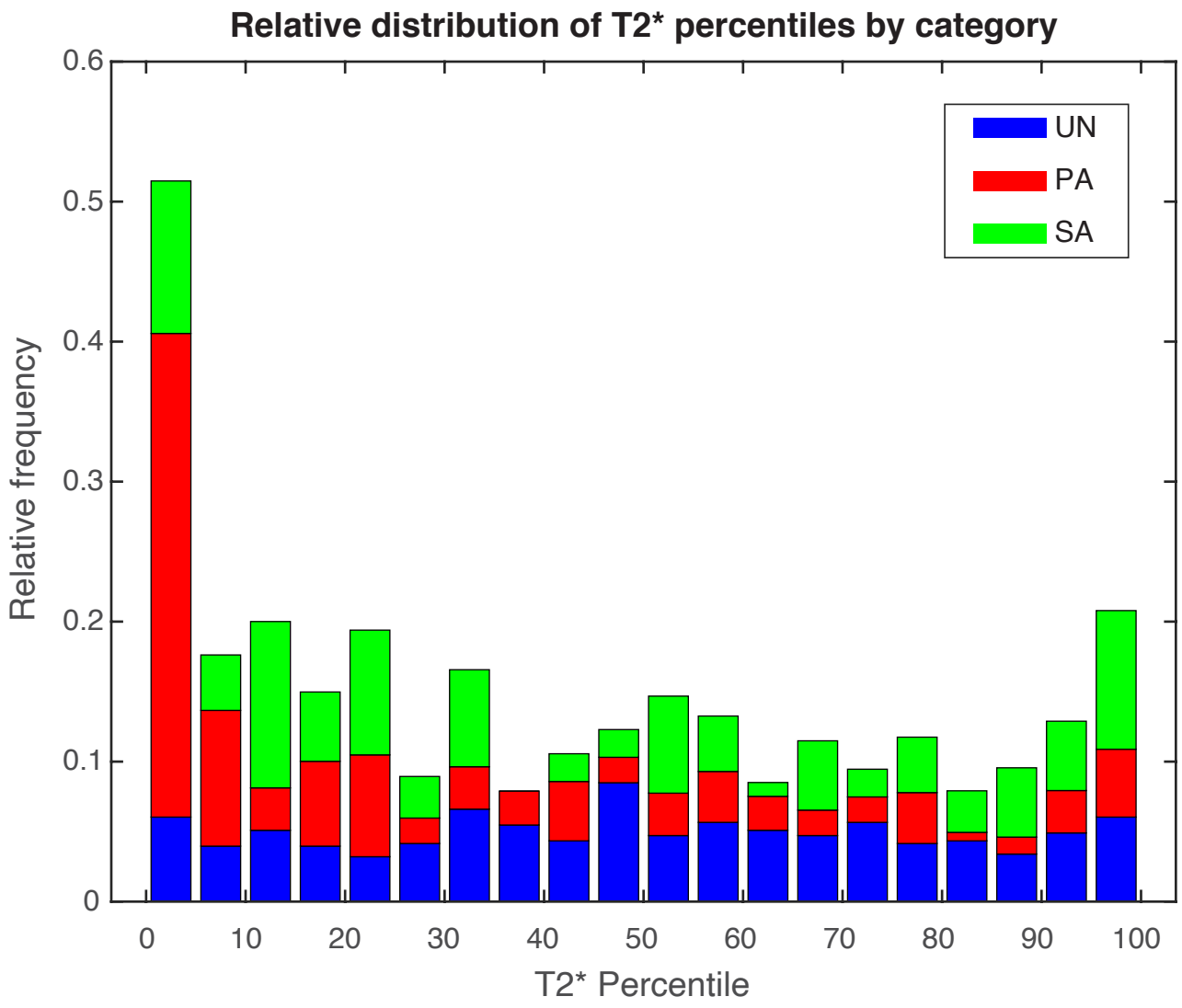
Relative distribution of T2* percentiles by category
UN
PA
SA
Relative frequency
0.6
0.5
0.4
0.3
0.2
0.1
0
0
10
20
30
40
50
60
70
80
90
100
T2* Percentile

Figure 5

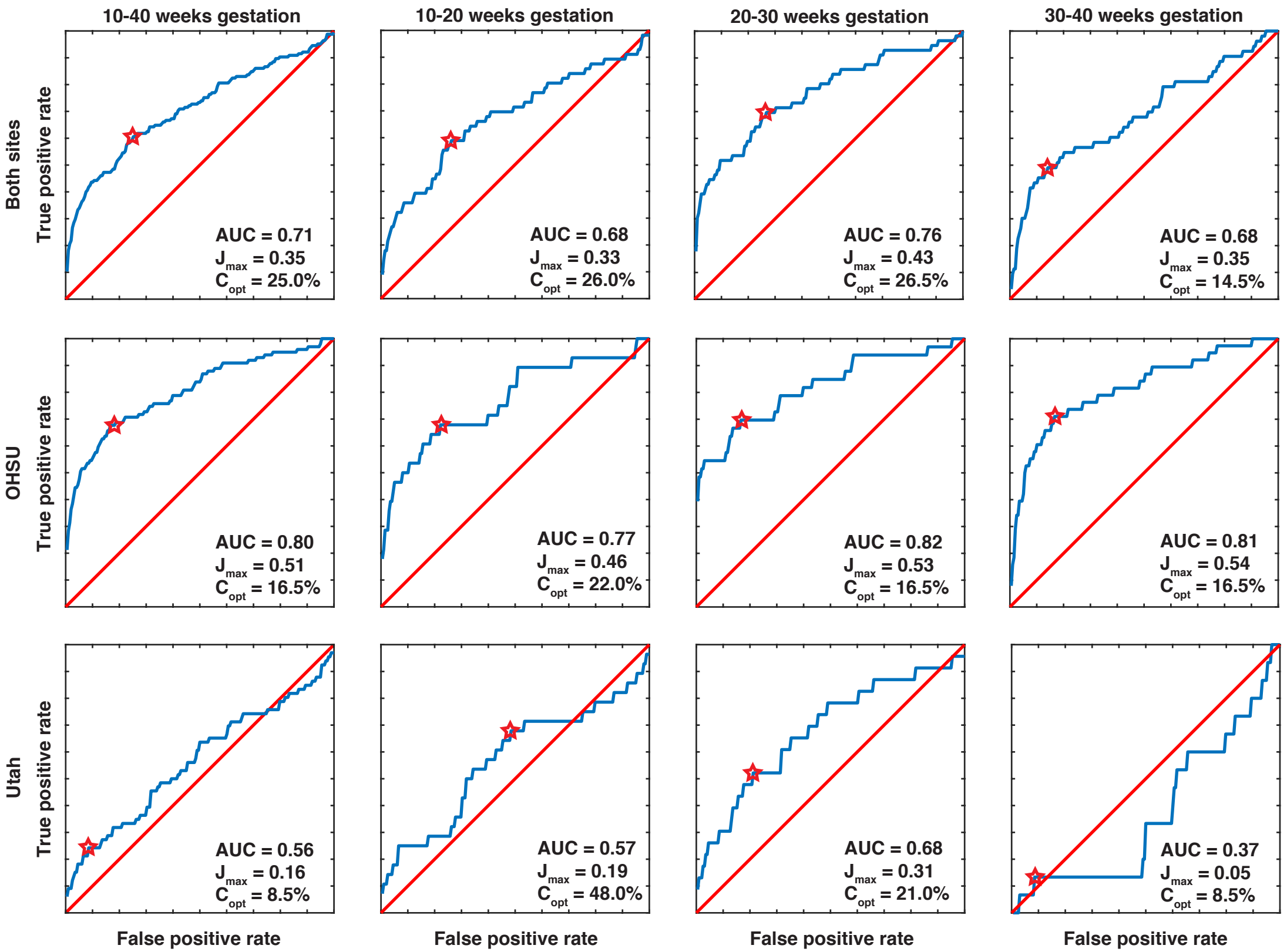
10-40 weeks gestation
10-20 weeks gestation
20-30 weeks gestation
30-40 weeks gestation
Both sites
OHSU
Utah
True positive rate
False positive rate
AUC = 0.71
J_max = 0.35
C_opt = 25.0%
AUC = 0.68
J_max = 0.33
C_opt = 26.0%
AUC = 0.76
J_max = 0.43
C_opt = 26.5%
AUC = 0.68
J_max = 0.35
C_opt = 14.5%
AUC = 0.80
J_max = 0.51
C_opt = 16.5%
AUC = 0.77
J_max = 0.46
C_opt = 22.0%
AUC = 0.82
J_max = 0.53
C_opt = 16.5%
AUC = 0.81
J_max = 0.54
C_opt = 16.5%
AUC = 0.56
J_max = 0.16
C_opt = 8.5%
AUC = 0.57
J_max = 0.19
C_opt = 48.0%
AUC = 0.68
J_max = 0.31
C_opt = 21.0%
AUC = 0.37
J_max = 0.05
C_opt = 8.5%

Figure 6

Figures

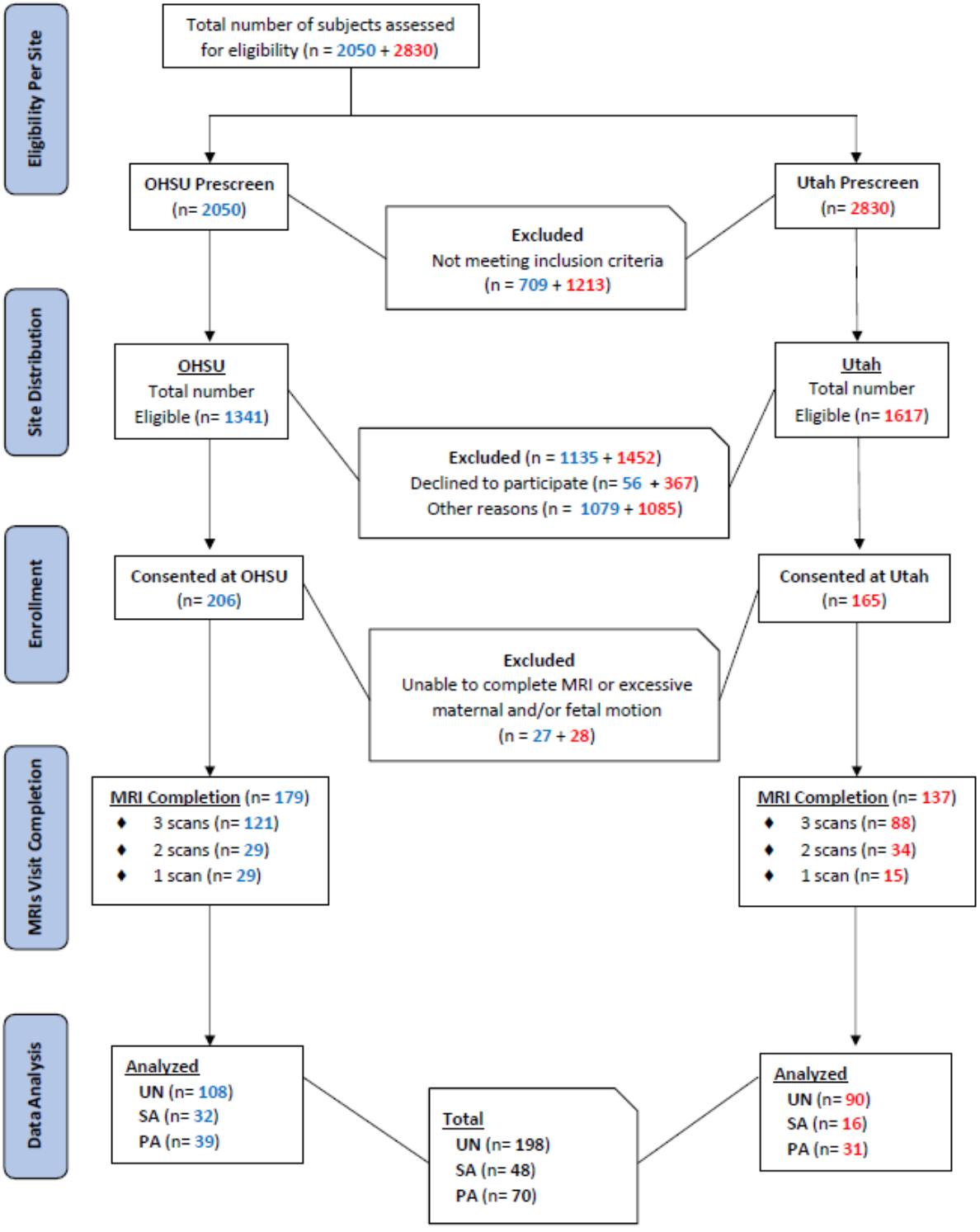

Figure 1

Enrollment flow chart. A flow chart detailing numbers of prospective patients screened, consented, and enrolled at both study sites, along with numbers of completed MRI studies meeting quality criteria for inclusion in data analysis presented here.

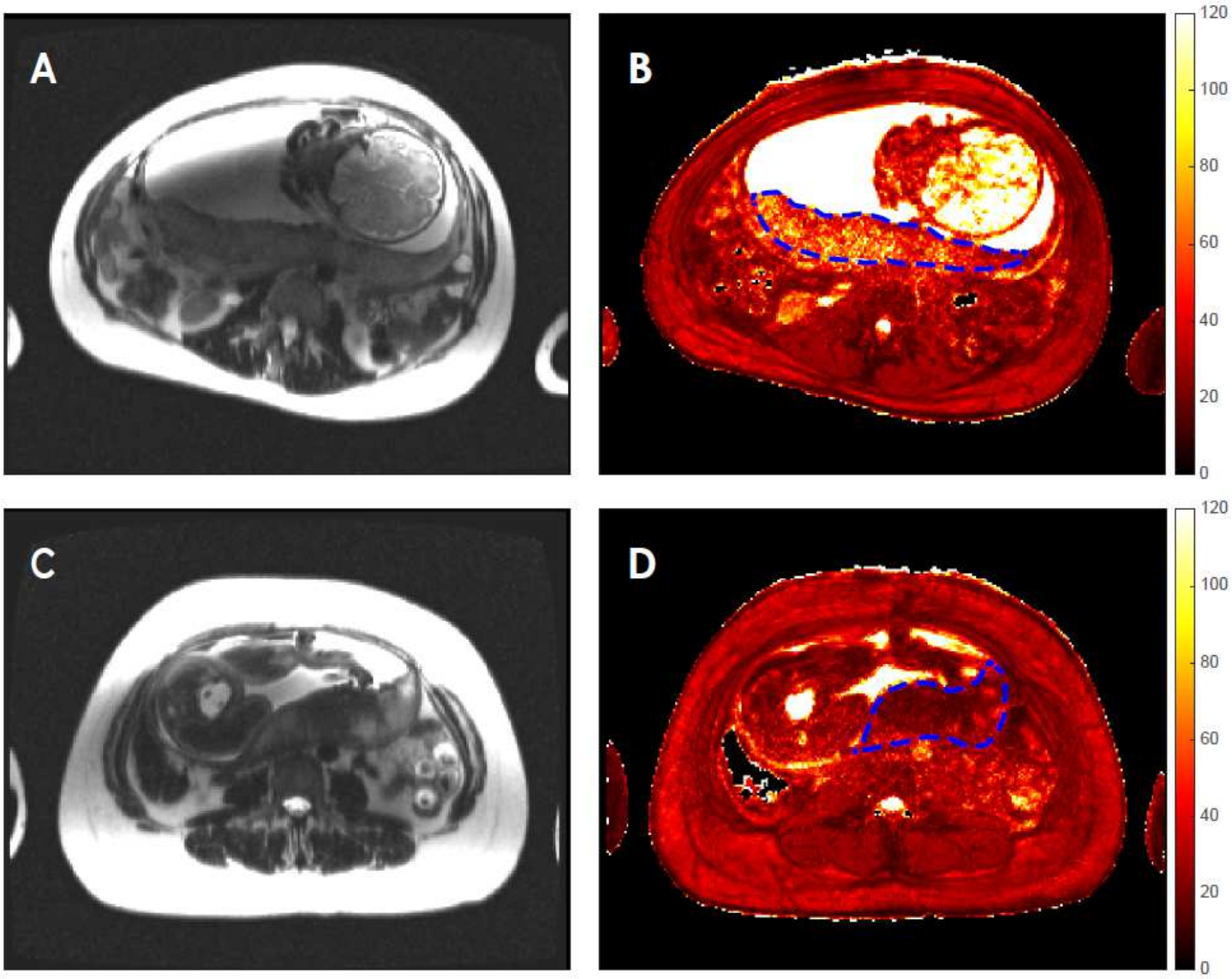

Figure 2

Comparison of anatomic imaging (T2-weighted HASTE, left column) and placental T2* mapping (right column) in a uncomplicated normal pregnancy at 232 days gestation (top row, panels A & B) with those from a primary adverse pregnancy at 235 days gestation presenting with severe preeclampsia (bottom row, panels C & D). The placenta is indicated by the dashed blue outlines overlaid on the T2* maps.

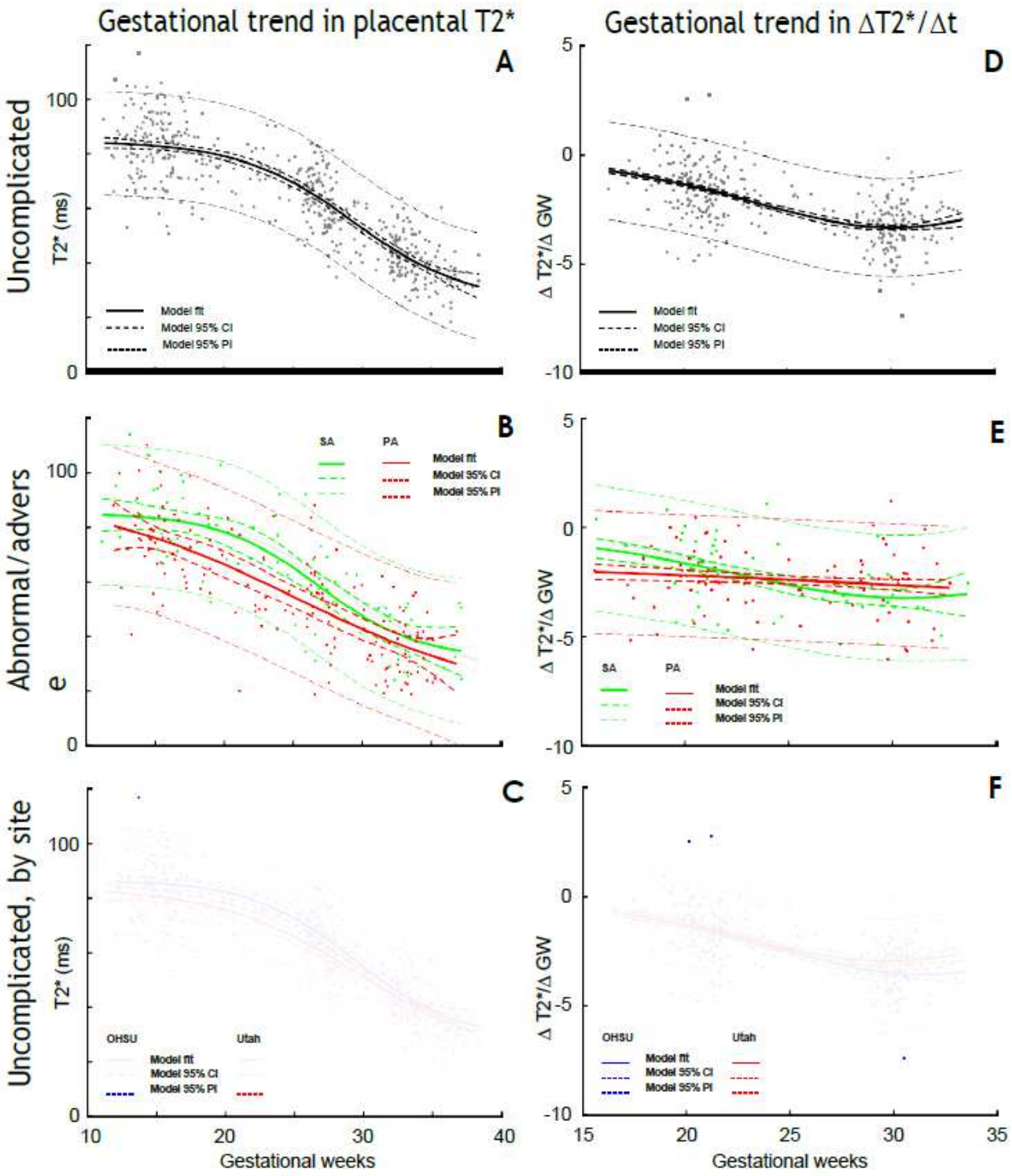

Figure 3

Gestational dependence of placental T2* values. Median T2* values for each completed study, computed over the entire placenta, are plotted as a function of gestational age at time of imaging in the three panels in the left column (panels A, B, C), while corresponding rates of change in placental T2* between repeated imaging time points within the same individual are plotted as a function of gestational age in the right column (panels D, E, F). The upper row plots these quantities for normal pregnancies, the middle row for

abnormal (green) and adverse (red) pregnancies, and the bottom row for normal pregnancies stratified by site (OHSU in blue, Utah in red). In all graphs, model regression curves (using the functions defined in Table 2) are indicated by the thick solid lines, the 95% confidence intervals by the dashed lines, and the 95% prediction intervals by the dot-dashed lines. The best fit and 95% CI curves from the plots in the upper row are shown in gray in the middle and bottom rows for reference.

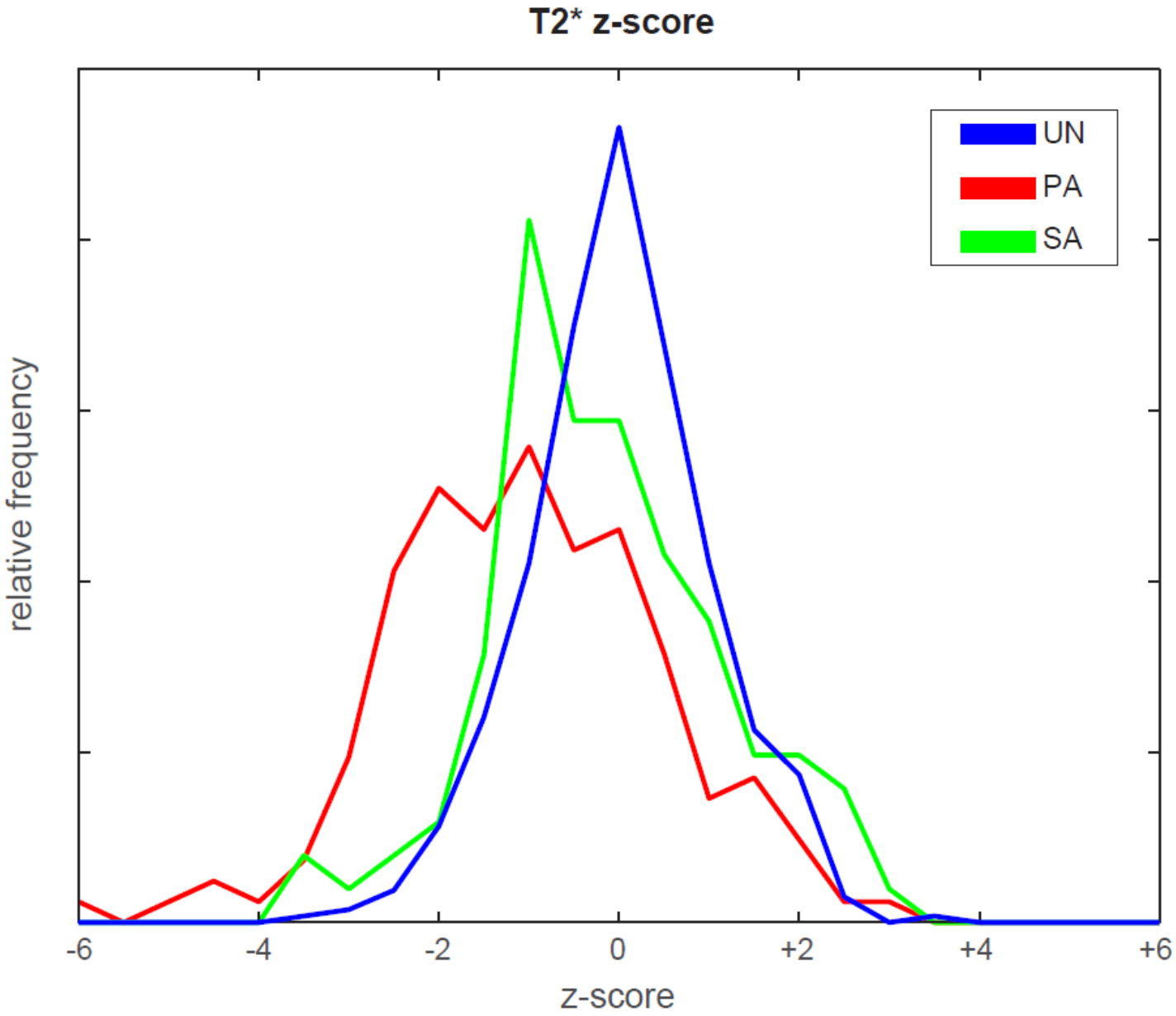

Figure 4

Histograms of T2* z-scores in normal, abnormal, and adverse pregnancies. Z-score histograms shown are computed using prediction intervals for sigmoid model regression to T2* measurements in UN pregnancies, applied to individual studies in UN (blue), PA (red), and SA (green) pregnancies.

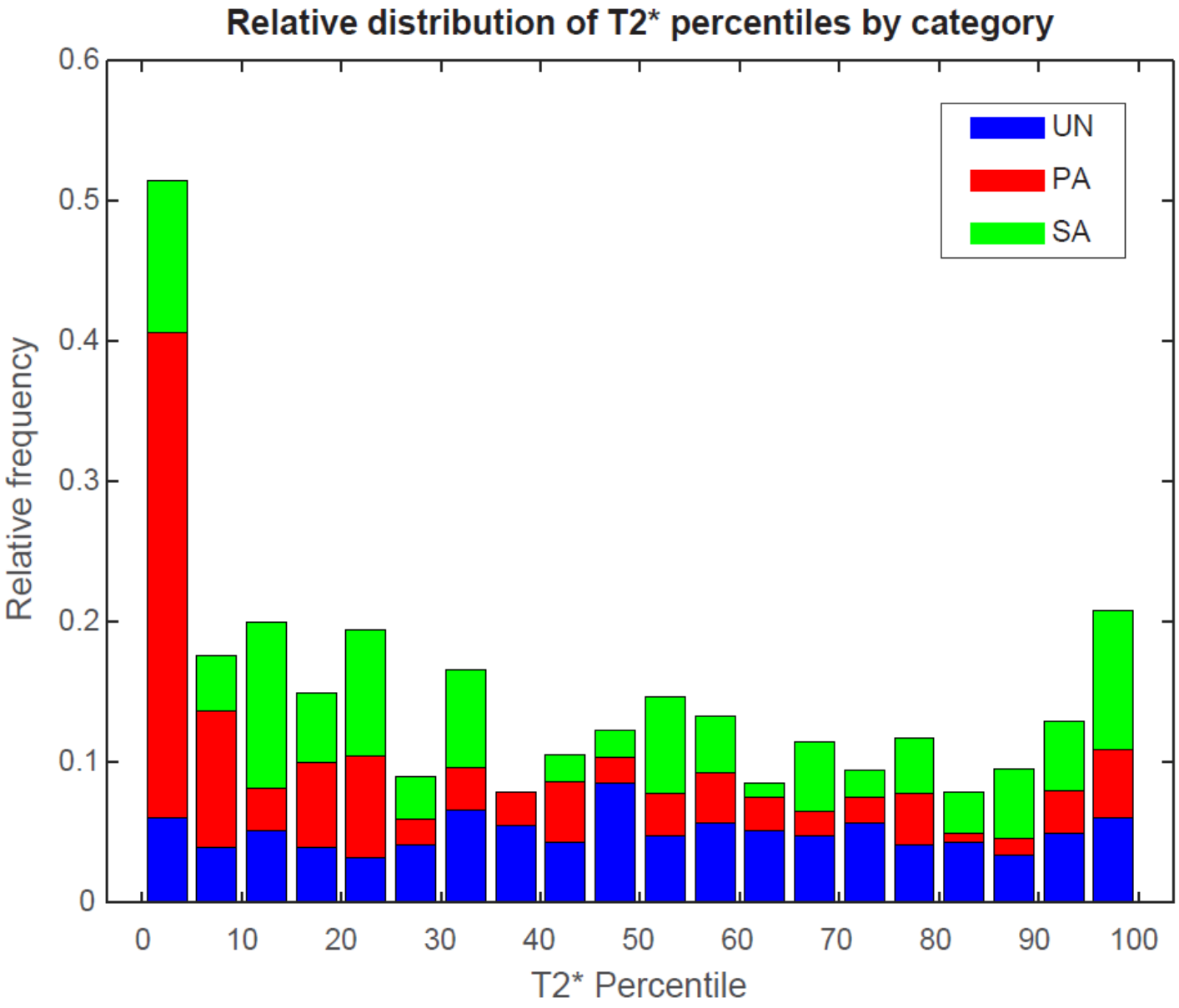

Figure 5

Bar chart of distribution of measured T2* percentiles for uncomplicated normal, primary adverse, and secondary abnormal pregnancies.

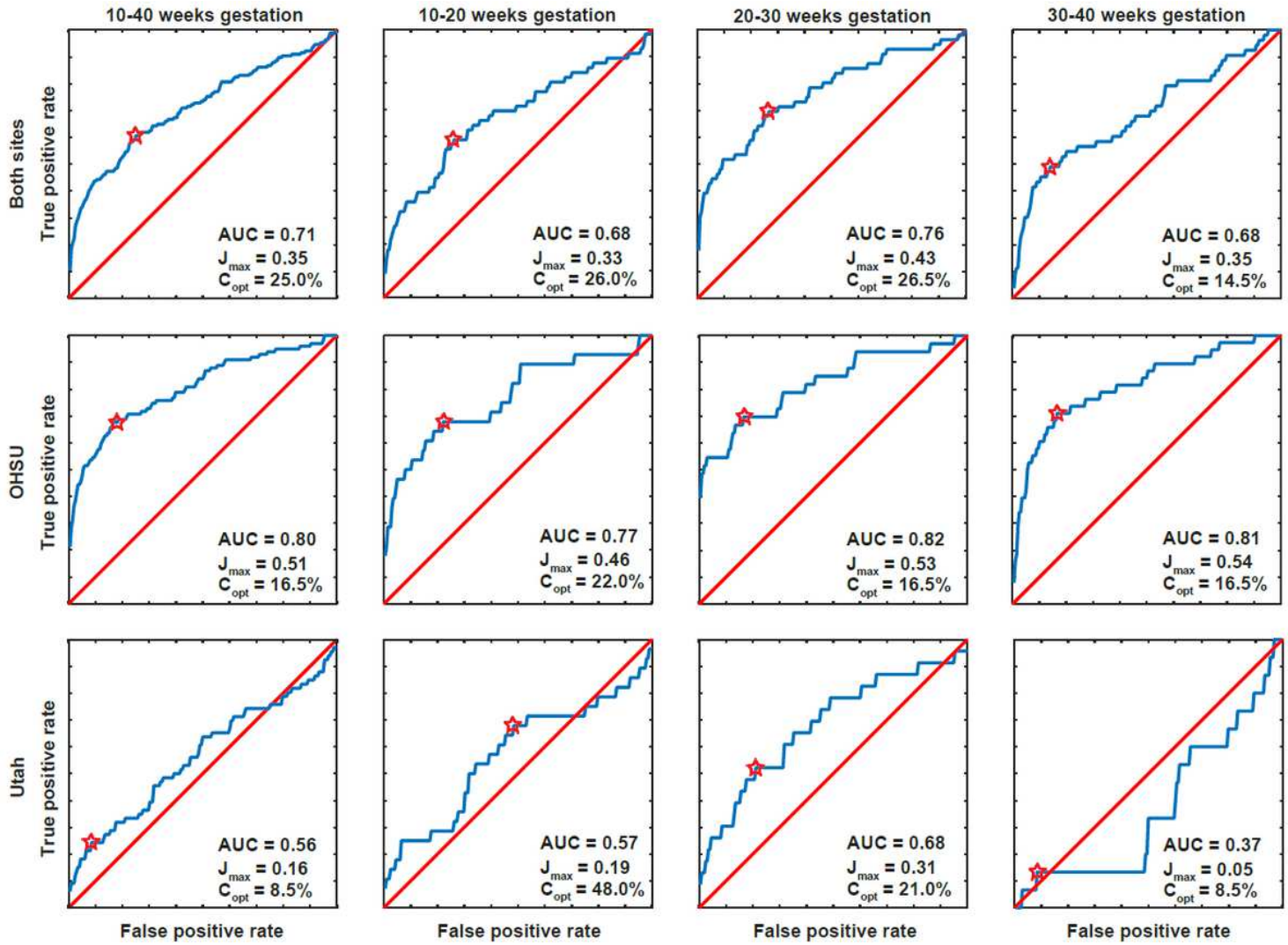

Figure 6

Receiver operator characteristic (ROC) curves for T2* measurements in pregnancies with our primary adverse outcome relative to uncomplicated normal pregnancies. The points where Youden's J is maximized are indicated by the stars. Area under the curve (AUC), J max, and the corresponding optimal cutoff threshold in T2* percentile relative to UN (C opt) are given in the figure legend for each panel.